Title page

A molecularly distinct cell type in the dmPAG regulates intermale aggression behaviors in mice

Chun-Yang Li[1,2], Cheng Miao[1,2], Jiaxing Wu[1,2], Yao Ge[2,3], Panpan Gao[1,2], Songlin Yin[1,2], Pei Zhang[2,3], Bo Tian[2,3], Wenqiang Chen[4]*, Xiao-Qian Chen[1,2]*

[1]Department of Pathophysiology, School of Basic Medicine, Tongji Medical College, Huazhong University of Science and Technology, Wuhan 430030, China. [2]Key Laboratory of Neurological Diseases, Ministry of Education, Wuhan, Hubei Province, 430030, China. [3]Department of Neurobiology, School of Basic Medicine, Tongji Medical College, Huazhong University of Science and Technology, Wuhan 430030, China. [4]Section of Integrative Physiology and Metabolism, Joslin Diabetes Center and Department of Medicine, Harvard Medical School, Boston, MA 02215, USA.

***Corresponding authors**: Xiao-Qian Chen; Wenqiang Chen
Email: chenxq@mails.tjmu.edu.cn (X.Q. Chen); Wenqiang.chen@joslin.harvard.edu (W. Chen)
Lead contact: chenxq@mails.tjmu.edu.cn (X.Q. Chen)

Author contributions: C.Y.L. researched, analyzed, interpretated data, and helped write the manuscript. C.M., J.W., Y.G., P. G., S. Y., P. Z., and B.T. researched data and helped analyze data. W.C. conceived and designed the study, interpretated data and wrote the manuscript; X.Q.C. secured the funding, designed the study, interpretated data, supervised all work and helped write the manuscript.

Acknowledgement: This work was funded by National Natural Science Foundation of China (No. 82173197 and 81972362 to X.Q.C. The authors thank Prof. Minmin Luo for kindly providing *Tac2*-Cre knock-in mouse line, Prof. Jian-Zhi Wang for kindly providing Ai9/tdTomato mice, and Prof. Yunyun Han for kindly providing suggestions on Ca^{2+} imaging. The authors gratefully thank the members from the X.Q. Chen Lab help with this project during the first-wave of COVID-19 in Wuhan.

Competing Interest Statement: The authors declare no competing interests.

Keywords: Periaqueductal gray, Tachykinin, Aggression, Translating ribosome affinity purification, Chemogenetics

Graphic Abstract

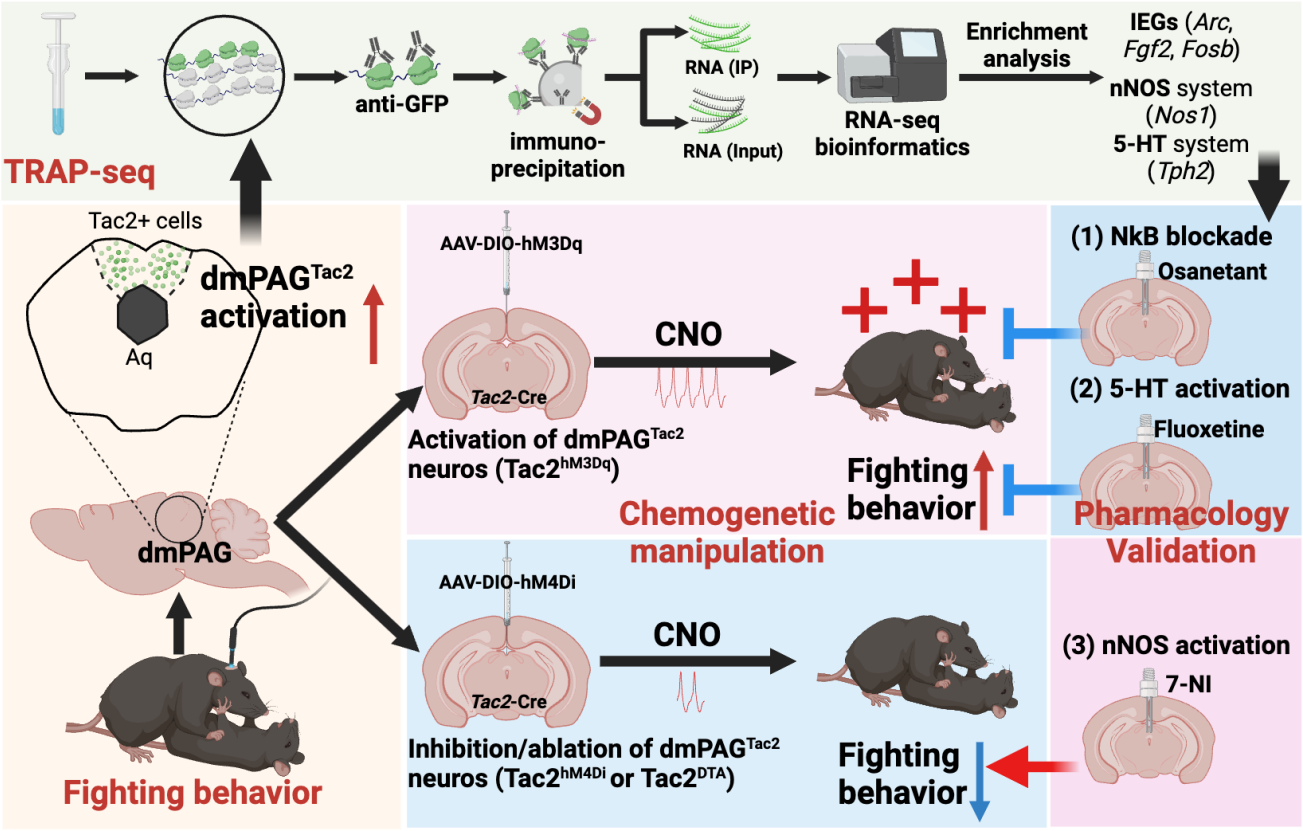

Abstract

The periaqueductal gray (PAG) has been suggested as a central hub for defensive responses to threatening stimuli and regulation of aggression. However, little is known on the circuitry and molecular mechanisms that govern this regulation. Here, we investigate the role of a molecularly distinct cell type, *Taschykinin 2*-expressing neurons ($Tac2^{+}$), located in dorsomedial PAG (dmPAG), in modulating aggression in a mouse resident-intruder model. Using a rabies-assisted input mapping strategy, we found that $dmPAG^{Tac2}$ neurons received monosynaptic input from the ventromedial hypothalamus, a region implicated in mediating fighting behaviors. Whole-brain Fos mapping and *in vivo* Ca^{2+} recording in mice revealed that $dmPAG^{Tac2}$ neurons were exclusively activated by fighting behaviors. Further, we manipulated activity of $dmPAG^{Tac2}$ neurons using chemogenetic tools and found that activation of $dmPAG^{Tac2}$ neurons evoked, while inhibition or genetic ablation of $dmPAG^{Tac2}$ neurons suppressed fighting behaviors. To further reveal molecular pathways that govern this fighting behaviors, we profiled $dmPAG^{Tac2}$ neurons using a viral-based translating ribosome affinity purification (TRAP) approach and revealed that fighting behaviors specifically induced enrichment of serotonin-associated transcripts in $dmPAG^{Tac2}$ neurons. Last, we validated these findings by selectively delivering pharmacological agents into the dmPAG through guide cannula and reversed the behavioral outcomes induced by chemogenetic manipulation of $dmPAG^{Tac2}$ neurons. Collectively, we identify that $dmPAG^{Tac2}$ neuron as a molecularly distinct cell type that regulates mouse aggressive behavior in dmPAG region and thus suggest a novel molecular target for the treatment of exacerbated aggressive behaviors in populations that exhibit high-level of violence.

Introduction

The periaqueductal gray (PAG) is a conserved brain region located in the midbrain, well-positioned to form neural circuits for the regulation of a wide range of functions and behaviors such as respiration, fear, anxiety, prey, defense, and aggression (Carrive, 1993; Franklin, 2019; Linnman et al., 2012). Although traditionally considered as a downstream of key neural circuits related to defense and pain, the outputs of the PAG are connected directly to spinal nerves and muscles, and therefore the PAG is viewed as an integration center for processing upstream information (Chen et al., 2018; Motta et al., 2017; Silva and McNaughton, 2019). Early studies demonstrated that electrical stimulation of the PAG in cats directly elicited an aggressive-defensive response, known as "defensive anger", while lesions of the PAG blocked this response (Hunsperger, 1956; Hunsperger and Bucher, 1967). Electrical stimulation of the amygdala and the hypothalamus also induced aggressive responses, however, when these regions are lesioned, PAG stimulation still elicited robust aversive responses (Schreiner and Kling, 1953), suggesting that the PAG may play an independent role in eliciting aversive responses such as aggression and defense.

Functional activity-dependent studies also confirmed the critical roles of the PAG in regulating aggression and defense behaviors. Fos mapping in animals exhibiting aggression and defensive behaviors confirmed that PAG neurons were activated when exposed to a predator (Canteras and Goto, 1999) or predator odor (Dielenberg et al., 2001). More recently, studies using optogenetic stimulation, Ca^{2+} imaging, and electrophysiological recording of the PAG have affirmed the causal roles of the PAG in aggressive and defensive behaviors. Of note, many of these studies were conducted in subregions such as the dorsal PAG (dPAG) and the lateral PAG (lPAG) in a pan-neuronal manner (Deng et al., 2016; Lischinsky and Lin, 2020). However, there is a lack of understanding of whether anatomically and molecularly distinct cell type in the PAG that might play a role in regulating aggression and defense behaviors.

In this study, we focus on *tachykinin 2* (*Tac2*)-expressing neurons that are located in the dorsomedial PAG (dmPAG) and aim to reveal their critical roles in regulating aggressive responses using a resident-intruder (RI) paradigm in male mice. We revealed that this molecularly distinct cell type, namely, $dmPAG^{Tac2}$ neurons, not only exhibit unique expression pattern across the subnuclei of the PAG, but also receive monosynaptic inputs from the VMHvl, a known fighting center that has been suggested in regulating aggressive behaviors. Further, using bi-directional manipulation of neural activity in the $dmPAG^{Tac2}$ cells, we confirm that these cells play a key role of in regulating intermale aggression. Last, using translating ribosome affinity purification (TRAP)-based RNA-sequencing (RNA-seq), we identify the critical involvement of the neuronal nitric oxide synthase (nNOS) and serotonin (5-HT) systems, in modulating $dmPAG^{Tac2}$ neurons-mediated behavioral effects. Collectively, these findings show that the *Tac2*-expressing neurons serve as a molecularly distinct cell type in the PAG that regulates intermale aggression and thus suggesting that targeting these cells might help alleviate symptoms in humans exhibiting high levels of aggression and violence.

Results

Tac2-expressing neurons exhibit distinct expression pattern in the PAG

Previous studies reported that Tac2^{+} neurons are expressed in a wide range of brain areas including the amygdala, hypothalamus, nucleus accumbens, and spinal cord (Mar et al., 2012), however, their expression pattern in the PAG has not been characterized. To this end, we crossed *Tac2*-Cre knock-in mice with Ai9 reporter mice to selectively express tdTomato reporter protein in Tac2^{+} cells (Figure 1A). By aligning expression of Tac2^{tdTomato} cells to the Allen Brain Atlas (ABA), we confirmed that Tac2^{tdTomato} cells were located in highly selected brain areas such as the bed nucleus of the stria terminalis (BNST), hypothalamus, and amygdala (Figure 1B-C), consistent with previous reports (Mar *et al.*, 2012; Zelikowsky et al., 2018). In control mice (*Tac2*-Cre mice, Ai9 mice, and wide-type mice), no tdTomato^{+} cells were found (Figure S1A). In addition, we found that Tac2^{tdTomato} cells were enriched in the dorsal and ventral hippocampus (Figure 1C), although this expression pattern was not shown by the mRNA expression pattern from the ABA *in situ* hybridization (ISH) data.

We then specifically analyzed the expression pattern of Tac2^{tdTomato} cells in the PAG, and found that Tac2^{tdTomato} cells were expressed throughout the PAG (Figure 1D), consistent with the mRNA expression pattern noted in the ABA ISH data (Figure S1B). No tdTomato^{+} cells were found in the PAG of the control mice (Figure S1A). Analysis of the percentage of Tac2^{tdTomato} cells in the PAG revealed that Tac2^{tdTomato} cells were primarily located in the dmPAG (Figure 1E-F), to a level of 50% of the total numbers of *Tac2*-expressing cells in the pan-PAG areas. These data suggest that the PAG *Tac2*-expressing cells are mainly located in the dorsomedial subregion of the PAG.

dmPAG^{Tac2} neurons receive monosynaptic inputs from the hypothalamus

The unique anatomical expression pattern of Tac2^{+} cells in the dmPAG suggests that it could be a potentially ideal locus to receive synaptic inputs from various brain areas. Previous studies have identified several key brain areas involved in aggression behaviors, including the ventromedial hypothalamus (VMH) (Yamaguchi et al., 2020). We hypothesize that there is a direct connection between dmPAG^{Tac2} neurons to the VMH. To reveal the synaptic inputs projecting to dmPAG^{Tac2} neurons, we used a rabies viral (RV)-assisted adeno-associated virus (AAV)-based approach (de Jong et al., 2019; Wall et al., 2010) to map monosynaptic inputs onto the dmPAG^{Tac2} neurons across the whole-brain (Figure S2A). We confirmed the localization of the starter cells, as showed by cells both positive for mCherry (helper) and EGFP proteins (Figure S2B), were located in the dmPAG. Identification of GFP-expressing only cells throughout the brain was used to determine the anatomical locations and strength of synapses onto dmPAG^{Tac2} neurons (Figure S2C). We found that as expected, dmPAG^{Tac2} neurons mainly received synaptic inputs from the hypothalamus (Figure S2D), including the VMH and the lateral hypothalamus. Quantitative analysis confirmed that the VMH sent strong inputs (29.3%) to the dmPAG^{Tac2} neurons among several other identified brain areas (Figure S2E-F). In addition, we also found that neurons in the dorsal premammillary nucleus and the midbrain reticular nucleus directly synapse onto the dmPAG^{Tac2} neurons (Figure S2D), confirmed with a recent report (Wang et al., 2021).

dmPAG^{Tac2} neurons respond to aggression

Having characterized the specific anatomical features of dmPAG^{Tac2} neurons, including expression pattern and circuitry connection (Figure 1 and Figure S2), we next sought to determine the involvement of dmPAG^{Tac2} neurons in controlling fighting behaviors. First, we subjected the WT mice to a resident-intruder test (see *Methods*) and harvested brain tissues 90 min after fighting behaviors (Figure 2A). As expected, fighting behaviors activated neurons in a broad range of brain areas, including the paraventricular nucleus of the thalamus (PVT), periventricular zone (PVZ), anterior hypothalamic nucleus (AHN, Figure S3A-B). Focusing on the Fos^{+} neurons in the dmPAG, our results showed that, compared to the control mice kept at home cages, a significant number of Fos^{+} neurons were found in the dmPAG of the resident mice ($P < 0.0001$, Figure 2B-C). Of note, fighting behaviors also elicited an increased number of Fos^{+} neurons in the dmPAG of the intruder mice, when compared with the intruder control mice ($P < 0.001$, Figure 2B-C). In contrast, fighting behaviors had no significant effects in inducing c-Fos expression in other PAG subregions, such as dlPAG, lPAG, and vlPAG (Figure S3C).

We then investigated the role of dmPAG neurons in response to fighting behaviors using an *in vivo* fiber photometry. We injected an AAV vector carrying GCaMP6m (driven by hSyn promoter, neuron-specific) into the dmPAG of the WT mice that were implanted with a fiber above the dmPAG (Figure 2D). Correct placement of the fiber was verified by imaging of the reporter protein, enhanced green fluorescent protein (EGFP, Figure 2E). In addition, when subjected these mice to the resident-intruder test, we observed a large increase in Ca^{2+} transients in response to each attack bouts (Figure 2F-H). Notably, each attack elicited an increase in Ca^{2+} activity immediately after the start of the attack episodes and this increase returned to baseline level after the attack (Figure 2F). Thus, these results demonstrated the involvement of dmPAG neurons in fighting behaviors.

We further investigated the role of dmPAG^{Tac2} neurons in fighting behaviors in a cell type-specific manner, i.e., *Tac2*-expressing neurons in the dmPAG. We used a Cre-dependent AAV vector (Figure 2I) to label dmPAG^{Tac2} neurons and subjected the mice to the resident-intruder test (Figure 2J). Ninety minutes after the resident-intruder, we stained c-Fos staining in dmPAG^{Tac2} neurons, which were mCherry^{+} cells and confirmed that dmPAG^{Tac2} neurons were activated by fighting behaviors (Figure 2K). We then measured Ca^{2+} activity of dmPAG^{Tac2} neurons during the resident-intruder test. To this end, we injected a Cre-dependent AAV vector carrying GCaMP6m at Day 1 and performed the resident-intruder test at Day 21 (Figure 2L-M), similar to the paradigm with the WT mice described above (Figure 2A). Correct placement of the optic fiber was confirmed by imaging of the reporter EGFP protein (Figure 2N). Although the AAV vector targeted less neurons in *Tac2*-Cre mice than the WT mice (Figure 2N), we indeed observed an increase in Ca^{2+} activity in response to attack episode (Figure 2O-P) when these *Tac2*-Cre mice were subjected to the resident-intruder test. Taken together, these data suggest that dmPAG^{Tac2} neurons are involved in fighting behaviors.

Deletion or inhibition of dmPAG^{Tac2} neurons attenuates fighting behaviors

To further confirm the above observation that dmPAG^{Tac2} neurons respond to fighting behaviors, we next performed chemogenetic manipulations to examine the causal role of dmPAG^{Tac2} neurons in fighting behaviors.

First, we noted that the *Tac2*-Cre mouse line was originally generated by inserting a Cre-coding sequence in-frame with the *Tac2* coding sequence (Mar *et al.*, 2012), which suggests that this insertion might affect normal expression of the *Tac2* gene. Therefore, the resulting heterozygous *Tac2*-Cre mice are equivalent to half knockout (KO) of the Tac2 peptide. Thus, we performed a basic behavioral characterization of *Tac2*-Cre mice and their WT littermate controls. The results showed that *Tac2*-Cre mice exhibited similar levels of locomotor performances in the open-field test (Figure S4A-E) and social preference in the three-chamber social interaction test (Figure S4K-P). In the elevated-plus test, however, *Tac2*-Cre mice had increased time spent in the open arm, while the other measures were similar between the two groups (Figure S4F-J). Notably, *Tac2*-Cre mice had similar levels of fighting behaviors in the resident-intruder test (Figure S4Q-T), which establishes a non-different baseline level of fighting behaviors prior to our next genetic ablation and chemogenetic manipulation experiments.

We then sought to examine the behavioral effects of genetic ablation of dmPAG^{Tac2} neurons (Figure 3A-G). To this end, we injected a neuron-specific (hSyn promoter) Cre-dependent AAV vector encoding DTA-mCherry (Figure 3A-B) into the dmPAG of *Tac2*-Cre mice (*Tac2*^{DTA}). *Tac2*-Cre mice that received an injection of a Cre-dependent AAV vector encoding mCherry (Figure 3A-B) were served as the control (*Tac2*^{mCherry}). To confirm the efficacy of genetic ablation of dmPAG^{Tac2} neurons, we imaged the reporter protein mCherry in the dmPAG (Figure 3C) and verified that DTA-mediated ablation resulted in an 80% of ablation of dmPAG^{Tac2} neurons (Figure 3D), suggesting that this DTA ablation-based approach achieved a high efficiency in ablating *Tac2*-expressing cells in the dmPAG.

Prior to the viral injection, we established the baseline level of aggression in both two groups of mice. Three weeks after viral injection, we subjected these mice to the resident-intruder test again to test the effects of ablating dmPAG^{Tac2} neurons (Figure 3B). The results showed that *Tac2*^{mCherry} mice exhibited similar level of aggression during the resident-intruder test before and after AAV injection. However, mice with genetic ablation of dmPAG^{Tac2} neurons exhibited a significantly longer latency to attack (Figure 3E), decreased number (Figure 3F) and duration of attacks (Figure 3G), when compared not only to the baseline levels (i.e., prior to AAV injection, Figure 3B), but also to their *Tac2*^{mCherry} control mice. These data suggest that ablation of dmPAG^{Tac2} neurons attenuates aggression in male mice.

To further confirm the above results on genetic ablation of dmPAG^{Tac2} neurons, we examined the behavioral effects of chemogenetic silencing of dmPAG^{Tac2} neurons. First, we injected a neuron-specific (hSyn promoter) Cre-dependent inhibitory DREADDs (Designer Receptors Activated Only by Designer Drugs) vector, AAV-hSyn-DIO-hM4Di-mCherry, into the dmPAG of *Tac2*-Cre mice (Figure 3H-I, *Tac2*^{hM4Di} mice). In addition, *Tac2*-Cre mice that injected with a Cre-dependent AAV encoding mCherry construct served as the control (Figure 3H-I, *Tac2*^{mCherry}). Three weeks after the viral injection, we established the baseline level of aggression by administering *Tac2*-Cre mice with normal saline for 30 minutes, followed by the resident-intruder test (Figure 3J). Forty-eight hours later, these mice were administered with clozapine-N-oxide (CNO, 1 mg/kg, i.p.) for 30 minutes and subjected to the resident-intruder test again (Figure 3J). As expected, CNO administration failed to alter any measures of fighting behaviors, including latency to attack, number of attacks and duration of attacks in *Tac2*^{mCherry} mice (Figure 3K-N). However, the previously established fighting behaviors in the baseline test

were dramatically suppressed by CNO administration in *Tac2*^{hM4Di} mice, as showed by an increased latency to attack ($P < 0.01$, Figure 3L), decreased number ($P < 0.001$, Figure 3M) and duration of attacks ($P < 0.001$, Figure 3N). Notably, in *Tac2*^{hM4Di} mice administrated with CNO, the average numbers of attacks were reduced from an average of 10 to near zero. Of note, we chose to achieve chemogenetic inhibition using a relatively low dose of CNO (1 mg/kg) based on a previous report showing that CNO at higher doses (e.g., 5mg/kg) elicited non-specific response even in the absence of the DREADDs receptor expression (MacLaren et al., 2016). Indeed, we did not observe that chemogenetic inhibition of dmPAG^{Tac2} neuronal activity at the dose of 1 mg/kg had any obvious effects in altering locomotion in the open-field test (Figure S5A-D), whereas in the elevated-plus maze, except for an increase of time spent in the open arms (Figure S5F, see *Discussion*) after CNO administration, other measures for anxiety-like behaviors exhibited similar levels between the two groups (Figure S5E, G-H). In summary, the above results from either genetic ablation or chemogenetic inhibition suggest that ablation or inhibition of dmPAG^{Tac2} neurons can reduce aggression behaviors in male mice.

Activation of dmPAG^{Tac2} neurons elicits fighting behaviors

Having confirmed the necessity of dmPAG^{Tac2} neurons in fighting behaviors from either ablation or inhibition of these cells, we then performed chemogenetic activation experiment to test the sufficiency of dmPAG^{Tac2} neurons in fighting behaviors. We first expressed a neuron-specific Cre-dependent AAV encoding hM3Dq in the dmPAG of *Tac2*-Cre mice (Figure 4A-B, *Tac2*^{hM3Dq} mice). In control *Tac2*-Cre mice, we expressed a neuron-specific Cre-dependent AAV encoding mCherry construct (Figure 4A-B, *Tac2*^{mCherry}). To confirm the efficacy and specificity of chemogenetic activation of dmPAG^{Tac2} neurons, we intraperitoneally administered CNO at the dose of 0.5 mg/kg to examine c-Fos induction in Tac2^{+} cells (Figure 4C). The results showed that, 120 min after CNO administration, c-Fos induction was specific to hM3Dq-expressing neurons but not to mCherry-expressing neurons (Figure 4C-D). As a separate comparison, we intraperitoneally injected normal saline to *Tac2*-Cre mice expressed with either hM3Dq or mCherry and did not find evident c-Fos induction in either hM3Dq- or mCherry-expressing neurons (Figure 4C, showed by mCherry^{+}EGFP^{+} cells). Further double fluorescent staining confirmed that CNO administration resulted in a significantly increased percentage of mCherry^{+} cells in neurons that showed c-Fos induction ($P < 0.0001$, Figure 4D). Therefore, these results validated the efficacy and specificity of chemogenetic activation to dmPAG^{Tac2} neurons.

We next examined the behavioral outcomes of activating dmPAG^{Tac2} neurons. First, we established the baseline level of aggression by administering *Tac2*-Cre mice with normal saline for 30 minutes and subjected them to the resident-intruder test. Forty-eight hours later, these mice were administered with CNO (0.5 mg/kg, i.p.) for 30 minutes and subjected to the resident-intruder test again (Figure 4E). The results showed that, upon CNO administration, *Tac2*^{mCherry} mice had no behavioral changes in fighting behaviors, similar to the results of *Tac2*^{mCherry} mice from chemogenetic inhibition (Figure 3L-N). However, following CNO administration, *Tac2*^{hM3Dq} mice exhibited a significantly elevated levels of aggression towards the intruder mouse (Figure 4F-I), as showed by a decreased latency to attack ($P < 0.001$, Figure 4G), increased number ($P < 0.001$, Figure 4H) and duration of attacks ($P < 0.01$, Figure 4I). In addition, we tested the possible effects of CNO administration on other behavioral performances, and failed to observe any obvious effects of chemogenetic activation of

dmPAG^{Tac2} neuron in altering locomotion in the open-field test (Figure S6A-D) and anxiety-like behaviors in the elevated-plus maze (Figure S6E-H). In summary, these results suggest that activation of dmPAG^{Tac2} neurons elicits fighting behaviors and increases aggression in male mice without producing obvious effects in the other behaviors tested.

Fighting behaviors alters transcriptional profiles in dmPAG^{Tac2} neurons

The above data demonstrate that dmPAG^{Tac2} neurons not only are involved, but also play a causal role in fighting behaviors in a resident-intruder paradigm. We next sought to reveal the molecular profiles in dmPAG^{Tac2} neurons that altered by fighting behaviors. To this end, we performed a translating ribosome affinity purification (TRAP) by injecting an a Cre-dependent AAV vector with eGFP-tagged ribosome protein L10 (AAV-EF1a-FLEX-EGFPL10a, Figure 5A-B) in the dmPAG of male *Tac2*-Cre mice. These mice were subjected to the resident-intruder test or were maintained as home-cage controls (Figure 5C, see *Methods*). Sixty minutes after the test, we immediately collected brain tissues containing the dmPAG and performed TRAP. Ribosome-associated mRNAs specific to dmPAG^{Tac2} neurons were purified and RNA-sequencing (RNA-seq) were performed (see *Methods*). By comparing gene expression between the two groups of immunoprecipitated IP samples (RI vs Control), we identified 58 differentially expressed genes (DEGs) induced by fighting, including 34 upregulated DEGs and 23 downregulated DEGs (Figure 5D). KEGG analysis showed that, the pathways impacted by fighting behaviors mainly involved inflammation, immunity and infection-related pathways (Figure 5E-F). Of note, estrogen signaling pathway, which has been shown previously in controlling inter-male aggression behaviors in the VMH (Hashikawa et al., 2017), was identified by our KEGG analysis, consistent with the previous notion that estrogen can regulate aggression behaviors in rodents (Dombret et al., 2020; Jager et al., 2018; Sano et al., 2013).

To identify novel targets that might play a critical role in fighting behaviors, we performed enrichment analysis (Zhao et al., 2017) by calculating fold-enrichment (RI-IP/Ctr-IP) and aligned the top candidate genes (Figure 5G) based on their enrichment score. The analysis showed that, among the most significantly enriched genes, several well-established immediate-early genes, including *Arc*, *Egr1*, *Fgf2*, and *Fosb*, were highly upregulated, suggesting that, indeed, dmPAG^{Tac2} neurons were activated by fighting behaviors and that the TRAP-seq approach was accurate in capturing these molecular events. In downregulated genes that enriched in dmPAG^{Tac2} neurons suppressed by fighting behaviors, we identified *Nos1*, a neurotransmitter gene that was previously reported to interact with the 5-HT system and to play a critical role in aggression behaviors (Carreno Gutierrez et al., 2020). Venn plot shows that *Nos1* was a common DEG gene that its expression was suppressed by resident-intruder, not only in the RI and Ctr comparison among the IP samples, but also in the IP and INPUT comparison among the RI groups (Figure H), suggesting that *Nos1* was related to both attacks and Tac2 signaling, thus it could be a potential target in dmPAG^{Tac2} neurons to regulate fighting behaviors. In downregulated genes showed enrichment in dmPAG^{Tac2} neurons, we identified *Tph2*, a gene encoding tryptophan hydroxylase 2, a rate-limiting enzyme that is primarily expressed in the serotonergic neurons of the brain, to be a potential target in dmPAG^{Tac2} neurons to regulate fighting behaviors, which is consistent with previously established knowledge that the serotonergic system is involved in aggression at both ligand and receptor levels (Coccaro et al., 2015; Olivier and Mos, 1992; Olivier and van Oorschot, 2005; Vazquez-Leon et al., 2023). Our secondary analysis by calculating

fold change as IP/Input (RI) when normalized by IP/Input (control) also revealed that *Nos1* and *Tph2* were highly enriched in this fold-change analysis (Figure 5I). Thus, we selected *Nos1* and *Tph2* for the subsequent validation experiment.

Pharmacological manipulation of dmPAG^{Tac2} neurons in fighting behaviors

To validate the potential molecular pathways in dmPAG^{Tac2} neuron altered by fighting behaviors, we first tested the involvement of the neurokinin B (NkB) signaling. *Tac2* (TAC3 in human) encodes neurokinin B (NkB) and is involved in neurotransmission and neuromodulation in the brain (Andero et al., 2014). The *Tac2* product, NkB, acts on its receptor NK3R to exert its downstream effects. Thus, we hypothesize that NkB/NK3R is required for eliciting fighting behaviors in dmPAG^{Tac2} neurons. To this end, we pharmacologically blocked the NkB/NK3R signaling by administering an Nk3R antagonist, Osanetant, through a guide cannula to target the dmPAG in mice receiving chemogenetic activation of dmPAG^{Tac2} neurons (Figure 6A; Figure S7A). First, we reanalyzed the TRAP-seq data and found a mild increase of *Tac2* expression in mice subjected to resident-intruder when compared to their home-cage controls (Figure S7B-C). Second, in pharmacological blockade experiment, as expected, in these Tac2^{hM3Dq} mice, CNO administration significantly elicited fighting behaviors (Figure 6B-D), consistent with our previous findings (Figure 5F-I). Fighting behaviors in chemogenetically activated mice were effectively attenuated by intra-dmPAG delivery of Osanetant, as showed by a significant increase in latency to attack ($P < 0.05$, Figure 6B) and decreased number of attacks ($P < 0.05$, Figure 6C), whereas the duration of attacks showed a trend of decrease (Figure 6D, $P = 0.186$). Nevertheless, our data demonstrate that blockade of the NkB/NK3R signaling can attenuate fighting behaviors elicited by activation of dmPAG^{Tac2} neurons, suggesting that the Tac2/NkB/NK3R axis is a potential pathway to intervene the exaggerated aggression.

Having established the involvement of the NkB/NK3R signaling pathway itself in the expression of fighting behaviors, we next sought to validate the two targets identified by TRAP-seq, namely, *Tph2* and *Nos1*. *Tph2* gene encodes tryptophan hydroxylase 2, which mainly acts as a rate-limiting enzyme of 5-HT synthesis to increase the levels of 5-HT (Jones et al., 2020). Since our previous TRAP-seq identified that *Tph2* is one of the downregulated genes in dmPAG^{Tac2} neurons when mice were subjected to the resident-intruder test, we hypothesize that intervening 5-HT reuptake thereby increasing 5-HT levels in the extracellular synaptic cleft, as previously demonstrated (Bianchi et al., 2002; Malagie et al., 1995), could be a means to block the behavioral effects induced by chemogenetic activation of dmPAG^{Tac2} neurons. To this end, we intracranially delivered fluoxetine, a widely used selected 5-HT reuptake inhibitor, into the dmPAG prior to chemogenetic activation (see *Methods*, Figure 6A). As expected, in these Tac2^{hM3Dq} mice, CNO administration effectively elicited fighting behaviors when compared to the baseline levels of aggression established by normal saline (Figure 6E-G). Intra-dmPAG delivery of fluoxetine, on the other hand, successfully prevented the chemogenetic activation-elicited fighting behaviors, as showed by a significantly increased latency to attack ($P < 0.01$, Figure 6E), decreased number ($P < 0.001$, Figure 6F) and duration of attacks ($P < 0.01$, Figure 6G), suggesting that targeting 5-HT reuptake in dmPAG neurons is sufficient to prevent the fighting behaviors elicited by activation of dmPAG^{Tac2} neurons.

We also tested the effects of targeting Nos1 in modulating fighting behaviors in mice. In our TRAP-seq data, we

identified *Nos1* as one of the most significantly downregulated candidates across multiple analyses (Figure 5G-I), suggesting that Nos1 might play a critical role in fighting behaviors. *Nos1* encodes nNOS (nitric oxide synthase), a major player of key functions not only in the cardiovascular system but also in the central nervous system (Forstermann and Sessa, 2012). An early study reported that mice with nNOS inhibition displayed exaggerated aggression behaviors, demonstrated by increased intensity of fighting behaviors upon i.p. administration of an nNOS specific inhibitor, 7-Nitroindazole (7-NI) (Demas et al., 1997). However, it is not studied whether nNOS signaling plays a role through dmPAG^{Tac2} neurons to induce aggression-like behaviors. We therefore hypothesize that nNOS inhibition could induce fighting behaviors through its action on dmPAG neurons. To this end, we administered 7-NI through a guide cannula to target dmPAG in mice receiving chemogenetic inhibition of dmPAG^{Tac2} neurons (Figure 6H). As expected, these Tac2^{hM4Di} mice showed significantly reduced fighting behaviors upon CNO administration, consistent with our previous observation (Figure 3L-N). However, targeted delivery of 7-NI into the dmPAG successfully abolished the effects of chemogenetic inhibition of dmPAG^{Tac2} neurons, as demonstrated by significantly shortened latency to attack ($P < 0.05$, Figure 6I), increased numbers ($P < 0.001$, Figure 6J) and duration of attack ($P < 0.01$, Figure 6K).

The above data suggest potential molecular mechanisms that underly dmPAG^{Tac2} neurons-mediated fighting behaviors. Specifically, we found that fighting behaviors induced a downregulation of *Tph2* gene in dmPAG^{Tac2} neurons, which both reflected by counts of transcripts and normalized fold changes (Figure S7D-E). We then further analyzed the TRAP-seq data mainly focused on 5-HT system-associated genes, including genes that encode 5-HT receptors. The analysis shows resident-intruder upregulated gene expression of 5-HT receptors (Figure S7F-G); thus, it suggests that a negative feedback mechanism, however yet unknown, might exist in 5-HT receptor system in dmPAG^{Tac2} neurons to regulate fighting behaviors (Figure S7H).

Discussion

dmPAG^{Tac2} neurons exhibit distinct expression pattern

Tac2^{+} neurons are distributed in the murine brain in a unique pattern. In the basal level, *Tac2* genes are expressed in a wide variety of brain areas associated with mood and social behaviors, including the BNST, medial habenular (MH), central amygdala (CeA) (Zelikowsky *et al.*, 2018). In pathological states such as prolonged social isolation, Tac2 can be strongly induced to act on the whole brain in a dissociable and region-specific manner (Zelikowsky *et al.*, 2018). The induction pattern of Tac2 peptide or distributed expression of Tac2^{+} neurons suggest that the regulatory roles of the Tac2/NkB signaling in multiple brain functions depend on its anatomical location and neural connection. The *Tac2*-expressing neuron located in the dorsomedial shell of the nucleus accumbens is previously characterized as a subtype of D1 medium spiny neurons to play a negative regulatory role in cocaine addiction (Zhao et al., 2022). In the CeA, *Tac2*-expressing neurons mainly modulate consolidation of fear memory (Andero *et al.*, 2014; Florido et al., 2021). A recent study showed that *Tac2*-expressing neurons in the BNST and the CeA regulate behavioral states, i.e., emotional valence, by sending inhibitory inputs to the LHA neurons expressing melanin-concentrating hormone (Fujita et al., 2021). These studies suggest that *Tac2*-expressing neurons are uniquely positioned in specific brain regions to modulate behavioral homeostasis.

In this study, we focus on *Tac2*-expressing neurons that are located in the dorsomedial portion of the midbrain. The PAG has been traditionally viewed as an integrating center for defensive responses, including panic, fight-flight and freezing behaviors (Deng *et al.*, 2016; Motta *et al.*, 2017). Early studies used c-Fos expression and observed that there was an anatomic segregation of defensive behaviors in the dorsal columns of the PAG (Vianna et al., 2003) and that the dmPAG is served as a relay station for acquiring aversive information to the other brain regions (Borelli et al., 2006). However, it is not clear which cell type mainly mediates this effect. Here, we uncovered that *Tac2*-expressing neurons in the dmPAG (dmPAG^{Tac2} neurons) are key neural substrates that play a critical role in intermale aggression. Using reporter mice (*Tac2*-Cre/Ai9^{tdTomato}), we revealed that in dorsal midbrain, Tac2 protein is predominantly expressed in the dmPAG (Figure 1D-F), consistent with the expression pattern of *Tac2* mRNA shown in the Allen Brain Atlas (Figure S1B). We further used rabies-assisted tracing and confirmed that dmPAG^{Tac2} neurons mainly receive monosynaptic inputs from the VMH (Figure S2D-F) and to a less extend from the cuneiform nucleus (CUN), two brain regions that are known involved in innate defensive behaviors and aggression (Bindi et al., 2023; Falkner et al., 2020; Zha et al., 2020). Previous studies have shown that the VMHvl-PAG projection conveys social signals during aggression, thus, we cannot exclude the possibility that dmPAG^{Tac2} neurons might be involved in these midbrain circuits in a projection-specific manner to regulate the expression of aggression, which will be an interesting topic for future studies.

dmPAG^{Tac2} neurons are recruited during intermale aggression

Due to the fact that *Tac2*-expressing neurons in the PAG are mainly located in the dmPAG (Figure 1D-F) and that they are mainly receiving direct inputs from the VMH (Figure S2D-F), we hypothesize that dmPAG^{Tac2} neurons are involved in aggression behaviors. Using a resident-intruder paradigm, indeed we found that fighting

behaviors not only activate dmPAG neurons, but also specifically activate dmPAG^{Tac2} neurons, which are shown by induction of c-Fos protein (Figure 2B-C, 2K) and time-locked Ca^{2+} transient examined by fiber photometry recording (Figure 2F-H, 2N-P). These data suggest that dmPAG^{Tac2} neurons are recruited during aggression.

In clinical assessment, aggression behavior can be predominantly categorized into two major subtypes, impulsive aggression or premeditated aggression (Stanford et al., 2003), whereas in animal studies, no consensus has been made in categorizing aggressive behaviors (Fraser and Rushen, 1987). In rodents, several detailed descriptions of fighting types during aggression and defensive behaviors have been suggested in rodents, including play fighting, offensive aggression, defensive aggression, predatory aggression, and so on (Blanchard et al., 2003). These terms are intermingled in interpretation of behavioral tasks and might create confusion. One of the limitations of our study is, we mainly assess the role of dmPAG^{Tac2} neurons in intermale aggression, but not in other subtypes of aggressive behaviors such as maternal aggression, when a female defends the newborn pups (Miczek et al., 2001). Another distinct subtypes of aggression, predatory aggression, known as a pre-planned quite-biting attack towards a prey, for example, a cricket killed by a mouse, might also overlap with our intermale aggression. This is because, the PAG is known as a center in regulating predatory aggression (see a recent review (Zhao et al., 2023)), in which the lPAG mainly recruited for sensory processing (Yu et al., 2021) and the vlPAG glutamatergic neurons recruited for conditioned freezing responses (Tovote et al., 2016). However, whether dmPAG^{Tac2} neurons are directly or indirectly involved in predatory aggression is currently unknown and will be an interesting research topic for future study.

Bidirectional manipulation of dmPAG^{Tac2} neuronal activity alters fighting behaviors

Having confirmed the activation of dmPAG^{Tac2} neurons in intermale aggression during a resident-intruder test (Figure 2), we next ask whether bidirectionally manipulation of activity of dmPAG^{Tac2} neurons could alter the behavioral responses of fighting behaviors. Given that the insertion of Cre-Coding sequence might intervene *Tac2* gene expression in this knock-in mouse line we used (Mar *et al.*, 2012), we first compared the behavioral phenotypes of these *Tac2*-Cre mice and their WT littermates. Our results excluded that *Tac2*-Cre mice exhibit obvious abnormal behaviors in the open-field test, the three-chamber social interaction test and the resident-intruder test, except for that in the elevated-plus maze, *Tac2*-Cre mice spent a modest but significant increased time in the open arms (Figure S4K), an index represents anxiolytic-like behavior, similar to a previous report showing that prolonged social isolation causes anxiolytic-like behavior in the open-field test (Zelikowsky *et al.*, 2018). Similar to this finding, in our chemogenetic experiments, we similarly observed that CNO-induced inhibition of dmPAG^{Tac2} neuronal activity, resembling temporary loss of function of these cells, increased time spent in the open arms during the elevated-plus maze test (Figure S5F). All these data collectively suggest that the Tac2/NkB signaling might be a potential target for anxiety treatment. Nevertheless, our results in this baseline characterization contribute to the understanding of Tac2 peptide itself in behavioral regulation.

Our targeted inhibition and genetic ablation of dmPAG^{Tac2} neuronal activity yielded qualitatively similar results in the resident-intrude paradigm (Figure 3), which was showed by prolonged the latency to attack and significantly reduced numbers and duration of attacks, suggesting suppressed fighting behaviors. Thus, we

conclude that, dmPAG^{Tac2} neurons are necessary to mediate fighting behaviors. On the other hand, targeted chemogenetic activation of dmPAG^{Tac2} neuronal activity, however, not only shortened the latency to attack, but also significantly increased numbers and duration of attacks (Figure 4), demonstrating that activation of dmPAG^{Tac2} neurons is sufficient to induce fighting behaviors. These striking evidences show that dmPAG^{Tac2} neurons play a critical role in controlling fighting behaviors in male mice. In our chemogenetic manipulation experiment, we chose a controlled before-after study design, therefore to maximally measure the effect of various interventions on the same subjects, providing a better evaluation of variables at baseline and after interventions (Carey et al., 2012). The limitation of this design, however, is that the testing mice would be repeatedly exposed to an intruder mouse, which might cause sensitization to the stimuli. In fact, in clinics, people with high-level of violence and aggression would be very likely to exhibit high frequency of violent behaviors, i.e., physical attacks and verbal aggression towards multiple subjects (Caruso et al., 2021; Schablon et al., 2018). It would be intriguing, in the future, to investigate how transition from acute to repeated exposure of intruders alters dmPAG^{Tac2} neurons activity. Together, these data suggest that dmPAG^{Tac2} neurons regulate fighting behaviors in male mice while without affecting basic behavioral performance.

Role of nNOS and 5-HT systems in dmPAG^{Tac2} neurons during aggression

To investigate how dmPAG^{Tac2} neurons participate in fighting behaviors, we focus on the identification of signaling pathway in the dmPAG^{Tac2} neurons with TRAP-seq. We took advantage of a cell-type-specific mRNA purification from complex tissue or rare cell types, which enabled the assessment of rapid changes in translatomes in response to either endogenous or exogenous stimuli (Heiman et al., 2014), for instance, in our study, the resident-intruder. It is well-known that aggressive and violent behaviors both have ploygenic risk, meaning that there is a combined effect of multiple genetic influences on aggression (Kretschmer et al., 2023). However, the majority of the aggression studies in mice heavily rely on investigating individual gene risk and are limited to known candidate genes (Tecott and Barondes, 1996). Early studies have demonstrated that male mice with targeted mutation in gene for nNOS unexpected increase aggression behaviors towards a male intruder and induce excess sexual behaviors (mounting) towards a unreceptive female (Nelson et al., 1995). Male mice with mutation in gene for monoamine oxidase A (MAOA), on the other hand, also exhibited enhanced aggression, accompanied with altered amounts of brain 5-HT levels (Brunner et al., 1993; Cases et al., 1995). Likewise, mice lacking 5-HT_{1B} receptor exhibited more intense fighting behaviors towards an intruder (Saudou et al., 1994). Interestingly, the link between nNOS and 5-HT systems has also been demonstrated during aggression, showing that the nNOS KO mice exhibited impaired 5-HT turnover and deficient 5-HT receptor function (Chiavegatto et al., 2001). Despite all these early studies, over several decades ago, have pointed out a role of the nNOS and 5-HT systems in mediating intermale aggression and fighting behaviors, all of which have to be interpretated in the context of whole-body knockout of a specific gene product of interest. The secondary effect during germline or early postnatal development, however, cannot be neglected. Undoubtedly, there is an urgent need for a combinatory approach to uncover the neural basis of aggression.

Thus, in our study, after we identified the roles of dmPAG^{Tac2} neurons in regulating fighting behaviors, we sought to use TRAP-seq to identify a set of gene programs involved in fighting behaviors within the dmPAG^{Tac2} neurons.

Instead of studying the Tac2/NkB signaling or Tac2 peptide, we investigated the translational alteration of *Tac2*-expressing neurons in the dmPAG following resident-intruder exposure in mice that were prescreened for their aggressiveness. Our TRAP-seq approach not only accurately captures the immediate response of dmPAG^{Tac2} neurons to resident intruder, as showed by enrichment of IEGs such as *Fgf2*, *Erg1*, *Fosb*, *Arc* (Figure 5), but also enables us to specifically restrict on dorsomedial portion of PAG cells in a cell-type-specific manner. Thus, the spatial and temporal resolutions offered by TRAP-seq help identified the key players such as nNOS and 5-HT pathways. Ultimately, this approach has avoided the potential side effects or confounders that inevitably accompanied with whole-body loss-of-function study or Cre recombinase in the germline or during the early development stage.

With TRAP-seq, we identify that *Nos1* and *Tph2* are key substrates in dmPAG^{Tac2} neurons to regulate fighting behaviors. We argue that pharmacological manipulation of signaling pathways associated with these two genes, would efficiently induce or terminate fighting behaviors. Our validation experiment confirmed our TRAP-seq-identified targets (Figure 6) by showing that, on one hand, both pharmacological blockade of the Tac2/NkB/NK3R pathway with Osanetant and inhibition of 5-HT reuptake with fluoxetine, can suppress fighting behaviors elicited by activating dmPAG^{Tac2} neurons. On the other hand, inhibition of nNOS with 7-NI can successfully trigger fighting behaviors that are previously suppressed by chemogenetic inhibition of dmPAG^{Tac2} neurons. Thus, these results not only provide a validation to our targets identified with TRAP-seq, but also confirm with earlier reports showing that nNOS and 5-HT are indeed key players in intermale aggression (Brunner *et al.*, 1993; Cases *et al.*, 1995; Chiavegatto *et al.*, 2001; Nelson *et al.*, 1995; Saudou *et al.*, 1994). However, with more advanced techniques to manipulate neurons in a cell-type-specific manner at high temporal and spatial resolution, our data add novel insights into these existing literatures, thus further pinpoint the causal roles of the nNOS and 5-HT systems in fighting behaviors into a molecularly distinct cell type located in the dmPAG.

Of note, we did not validate other TRAP-seq-identified targets that also show a high enrichment to the dmPAG^{Tac2} neurons caused by resident-intruder. However, we cannot exclude the possibility that these targets expressed in the dmPAG^{Tac2} neurons might also play an important role in regulating fighting behaviors, which will be a topic of interest in future study. Also, as we discussed above, our present study is not mainly focused on revealing the circuit-associated mechanisms of fighting behaviors centered in dmPAG^{Tac2} neurons. Thus, future studies are need to further the involvement of VMH-projecting dmPAG^{Tac2} neurons in fighting behaviors.

Potential treatment for humans with exaggerated aggression

Uncontrolled aggression in humans has become a significant threat to the society, not only brings immediate physical harm but also causes chronic stress and pressure that might negatively affect one's mental health (Anderson and Bushman, 2002). In extreme cases, human aggression can evolve into incidents such as homicide or massive shooting (Fields, 2019). Thus, treating subjects to effectively control aggression behaviors are of high importance. In this study, we not only identify a molecularly distinct neuronal cell type in the midbrain that controls intermale aggression, but also uncover several druggable targets that could modulate exaggerated

aggressive behaviors. With these well-tolerated and commercially available pharmacological agents to correct aberrant aggression behaviors, our study further provides validity and new insights into potential treatments for mental illness patients with heightened aggression and violence.

Figures and Figure Legends

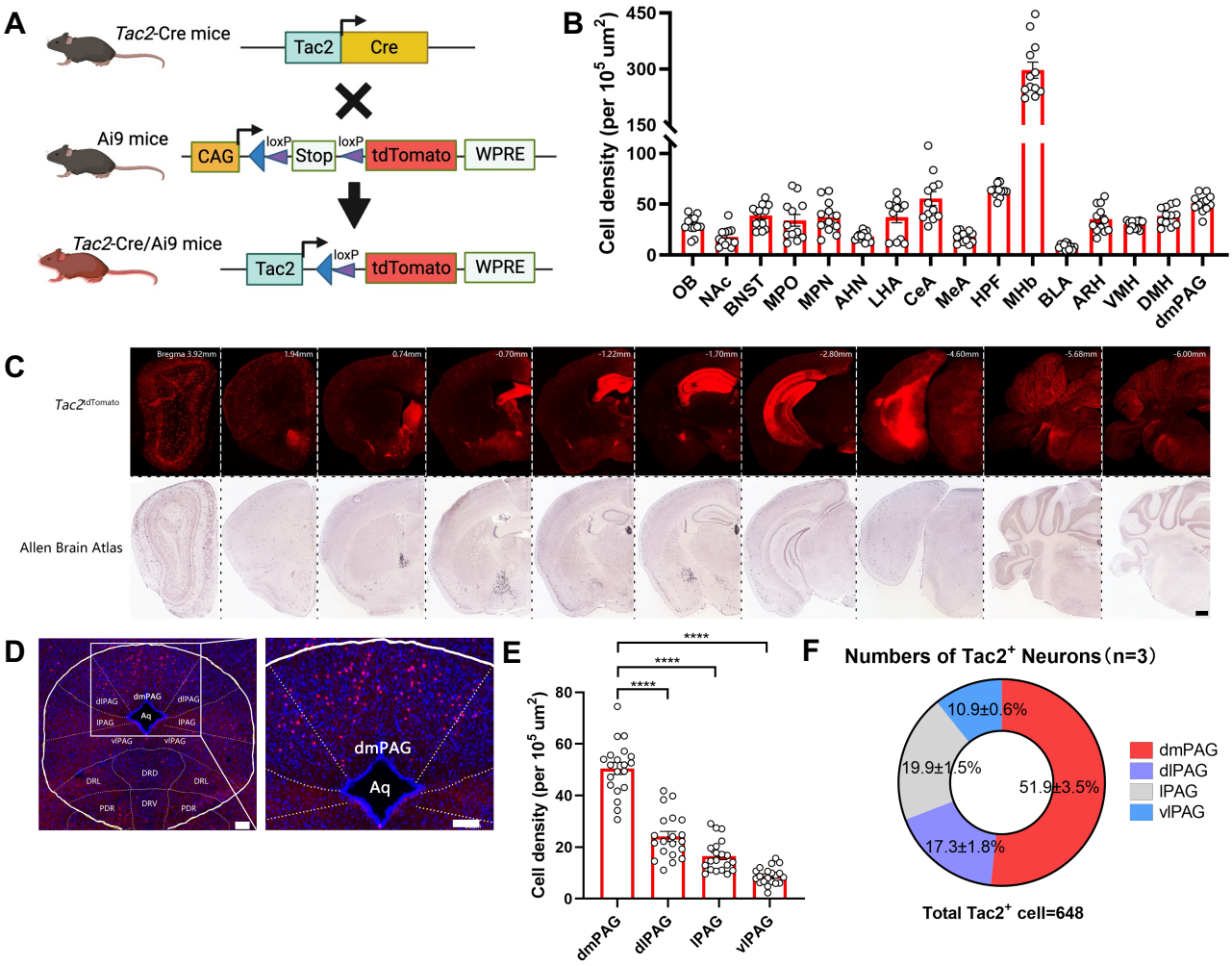

<u>Figure 1</u>. PAG *Tac2*-expressing neurons are mainly located in the dmPAG.

(A) Schematic showing mouse breeding strategy to selectively express tdTomato reporter in $Tac2^{+}$ cells. Schematic is created with BioRender.com. **(B)** Whole-brain expression analysis of density of $Tac2^{tdTomato}$ cells in different brain regions. Four series of representative images from N = 3 mice were analyzed. **(C)** Representative fluorescent images showing tdTomato-labeled $Tac2^{+}$ cells (red) in different coronal brain sections in *Tac2*-Cre/Ai9 reporter mice and in their respective Allen Brain Atlas images. Scale bar, 500 μm. **(D)** Representative fluorescent images showing distribution pattern of $Tac2^{+}$ cells in the PAG subregions. Scale bars, 1,000 μm (left panel) and 100 μm (right panel), respectively. **(E)** Analysis of expression pattern of $Tac2^{tdTomato}$ cells in different PAG subregions. Four series of representative images from N = 5 mice. **(F)** Pie chart showing numbers of $Tac2^{tdTomato}$ cells in different PAG subregions. N = 3 mice. Data were expressed as mean ± S.E.M. Significance was calculated by means of unpaired *t*-test. **** $P < 0.0001$.

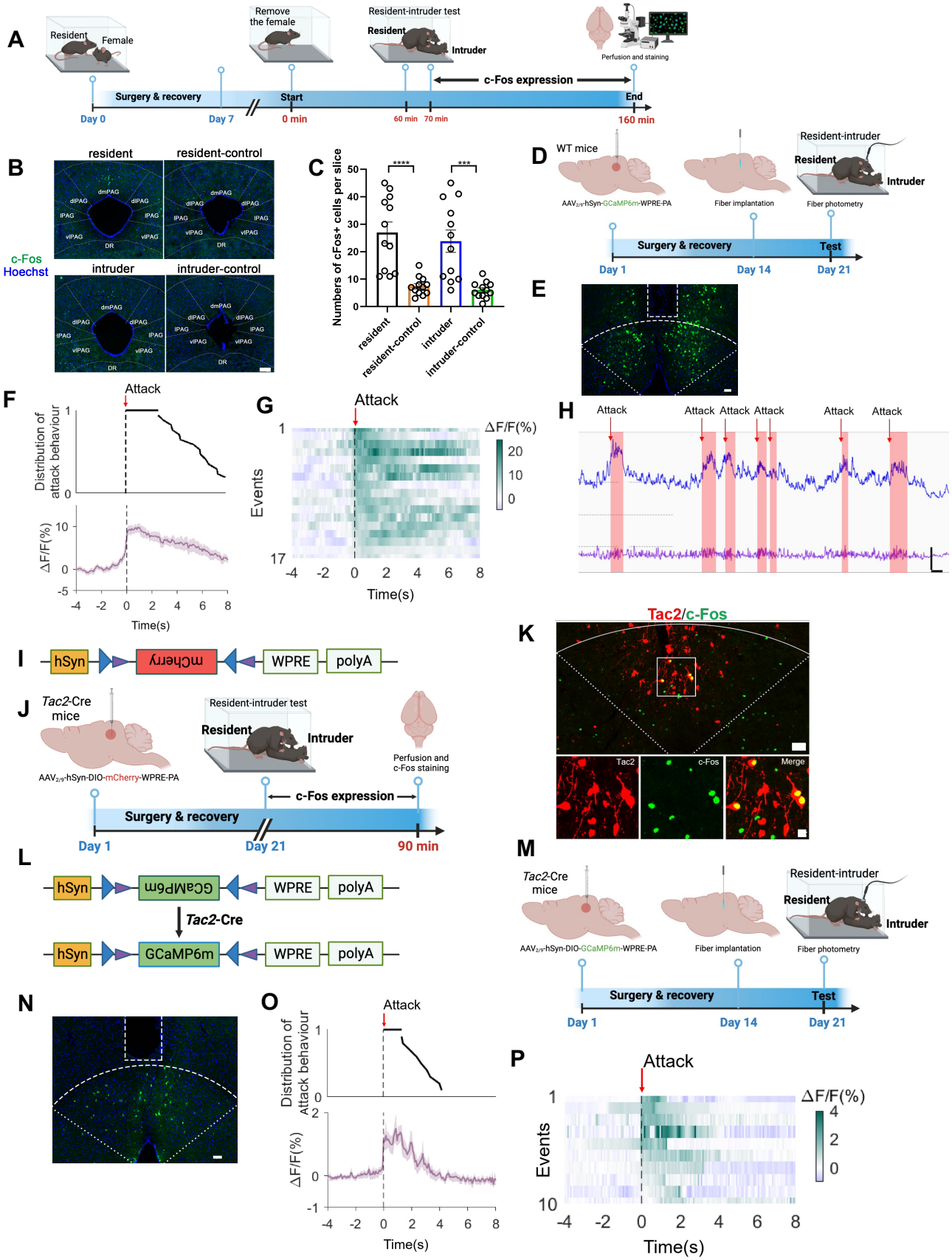

Figure 2. dmPAG^{Tac2} neurons respond to aggression

(**A**) Schematic showing strategy for mapping c-Fos expression in WT mice subjected to resident-intruder test. See ***Methods*** for further detailed procedure. (**B**). Upper panel: representative fluorescent images showing expression pattern of c-Fos^{+} cells in different subregions of PAG. Lower panel: representative fluorescent images showing expression pattern of c-Fos^{+} cells in different subregions of PAG (green: Fos; blue: Hoechst). Scale bar, 100 μm. (**C**)

Quantification of number of Fos^+ cells in dmPAG in WT mice. Data are presented as percentage of Fos^+ cells per slice (N = 3 mouse per condition). Data represent mean ± S.E.M. Significance was calculated by means of unpaired *t*-test. **** $P < 0.0001$. (**D**) Schematic showing strategy for *in vivo* fiber photometry in WT mice injected with an AAV-GCaMP6m vector driven by a hSyn promoter. (**E**) Representative fluorescent image showing fiber position targeting dmPAG region of WT mice. Scale bar, 50 µm. **(F)** Representative trace showing distribution of attach behavior synchronized with ΔF/F calculation. (**G**) Representative heatmap showing Ca^{2+} activity time-locked to attack episode, in which x-axis showing 4 seconds prior to and 8 seconds after the attack episode (labeled with red arrow). (**H**) Representative images showing one trial of Ca^{2+} activity in one representative WT mouse during resident-intruder test within a 5-min duration. Scale bar: 10s in x-axis and 2000 A.U. (fluorescence intensity) in y-axis. The bottom baseline indicates reference control channel (405 nm) and the upper traces indicate Ca^{2+} channel (470 nm). Red shaded areas indicate attack episodes and durations. (**I**) Vector information for expressing AAV-hSyn-DIO-mCherry. (**J**) Schematic showing strategy for assaying activation of $Tac2^+$ neuron by fighting behaviors. AAV vector was injected to *Tac2*-Cre mice to drive mCherry expression in $dmPAG^{Tac2}$ neurons. See ***Methods*** for further detailed procedure. (**K**) Representative images showing c-Fos expression (green) in $dmPAG^{Tac2}$ neurons (red mCherry labeled) in Tac2 mice subjected to resident-intruder test. Lower panels showing enlarged white box in the upper panel. Scale bars, 50 µm (upper panel), 20 µm (lower panel), respectively. (**L**) Vector information for expressing AAV-hSyn-DIO-GcaMP6m in *Tac2*-Cre mice. (**M**) Schematic showing strategy for *in vivo* fiber photometry in *Tac2*-Cre mice injected with a Cre-dependent AAV-GcaMP6m vector. (**N**) Representative fluorescent image showing fiber position targeting dmPAG region of Tac2 mice. Scale bar, 50 µm. (**O**) Representative trace showing distribution of attach behavior synchronized with ΔF/F calculation. (**P**) Representative heatmap showing Ca^{2+} activity time-locked to attack episode, in which x-axis showing 4 seconds prior to and 8 seconds after the attack episode (labeled with red arrow). Schematics (panel A, D, I, J, L, M) are created with BioRender.com.

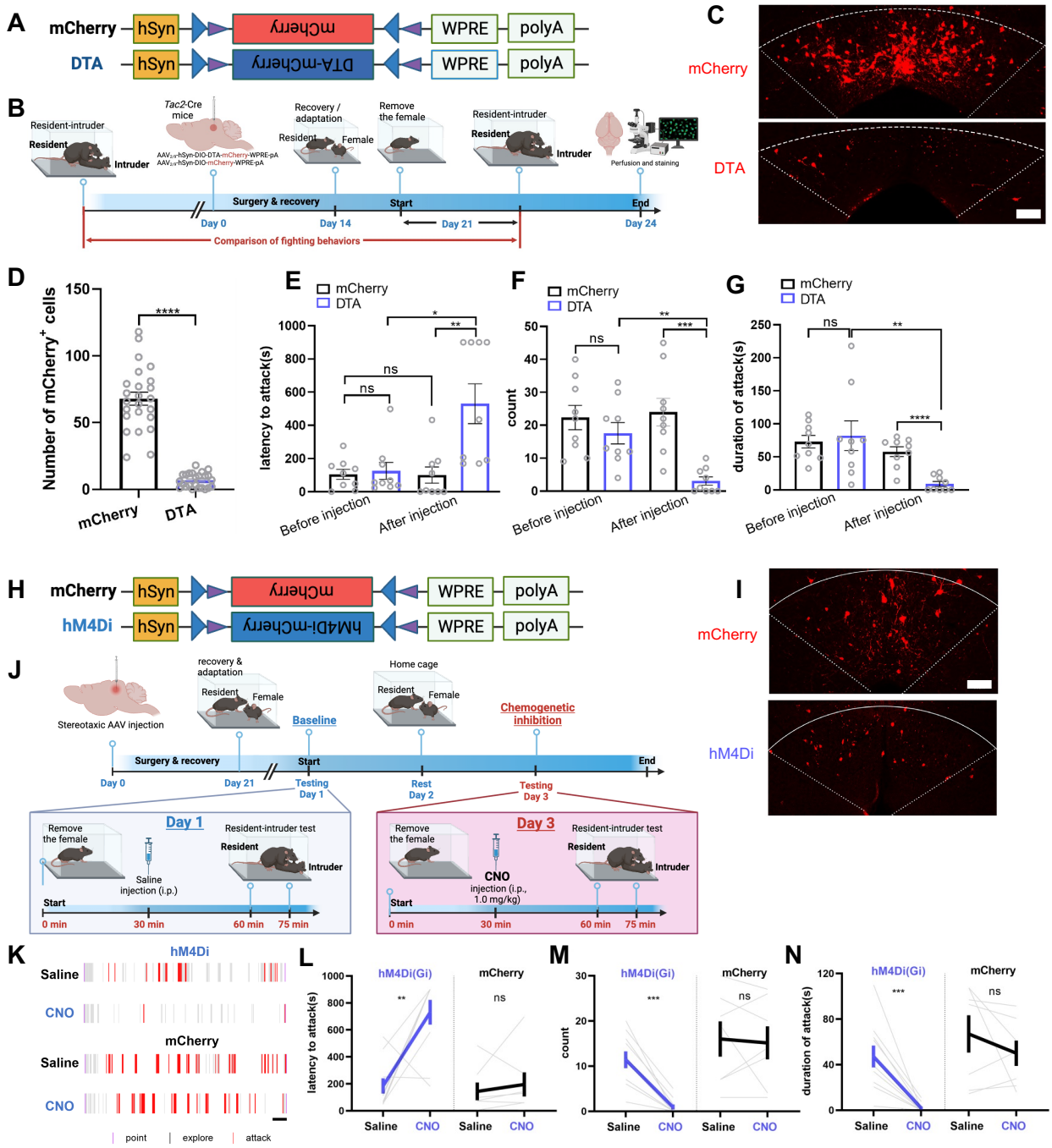

Figure 3. Ablation or inhibition of dmPAG^{Tac2} neurons suppresses fighting behaviors

(**A**) Vector information for expressing a Cre-dependent DTA vector or its control vector to dmPAG^{Tac2} neurons. (**B**) Schematic showing strategy for genetic ablation using AAV-hSyn-DIO-DTA-mCherry or AAV-hSyn-DIO-mCherry and the resident-intruder test. (**C**) Representative fluorescent images showing immunohistochemistry staining of mCherry (red) in dmPAG^{Tac2} neurons. (red: mCherry; Scale bar, 100 µm). (**D**) Quantification of number of mCherry^{+} cells in dmPAG in *Tac2*-Cre mice receiving injection of AAV-DIO-DTA or AAV-DIO-mCherry. Data are presented as percentage of mCherry^{+} cells per slice (N = 6 mice per condition). (**E-G**) Quantification of Latency to attacks (**E**), Number of attacks (**F**) and Duration of attacks (**G**). N = 9 in each condition. (**H**) Vector information for expressing a Cre-dependent hM4Di vector or its control to dmPAG^{Tac2} neurons. (**I**) Representative fluorescent images of hM4Di-mCherry or mCherry (both red; Scale bar, 100 µm) in dmPAG^{Tac2} neurons (red: mCherry; Scale, bar 100 µm). (**J**) Schematic showing strategy for resident-intruder test in *Tac2*-Cre mice injected with inhibitory DREADDs vectors. (**K**) Representative raster plots showing mouse attack (red bar) or exploring behavior (gray bar) during resident-intruder assay. Time scale, 1 min. (**L-N**) Quantification of Latency to attacks (**L**), Number of attacks (**M**) and Duration of attacks (**N**). N = 10 in *Tac2*^{hM4Di} group and N = 7 in *Tac2*^{mCherry} group. Data represent mean ± S.E.M. Significance was calculated by means of unpaired *t*-test. * $P < 0.05$, ** $P < 0.01$, *** $P < 0.001$, **** $P < 0.0001$. Schematics (panel A, B, H, and J) are created with BioRender.com.

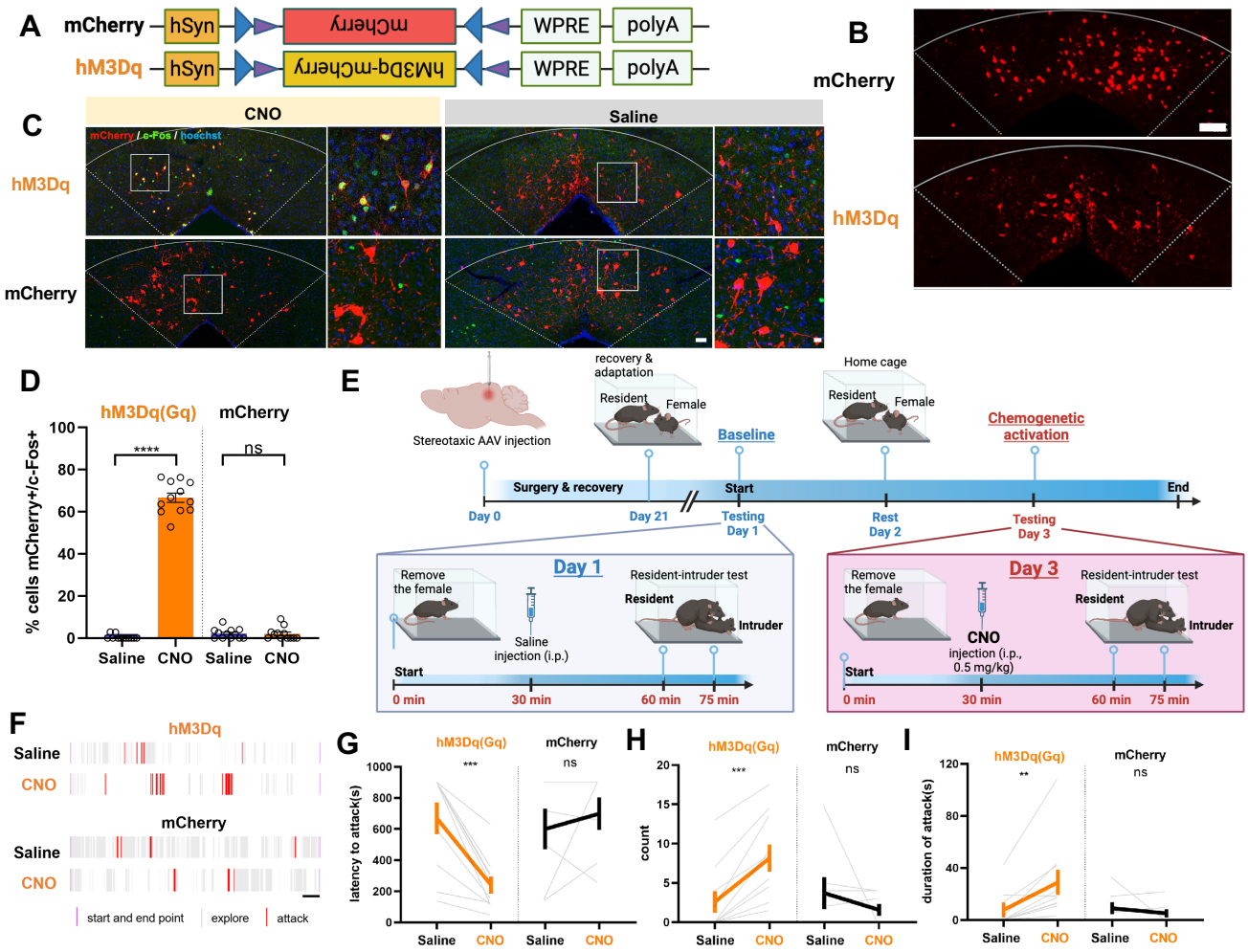

<u>Figure 4</u>. Chemogenetic activation of dmPAG^{Tac2} neurons elicits fighting behaviors

(**A**) Vector information for expressing a Cre-dependent hM3Dq vector or its control vector to dmPAG^{Tac2} neurons. (**B**) Representative fluorescent images of hM3Dq-mCherry or mCherry (both red) in dmPAG^{Tac2} neurons (red: mCherry; Scale bar 100 µm). (**C**) Representative fluorescent images showing double immunofluorescent staining of mCherry (red) and Fos (green) (red: mCherry; green: Fos; blue: Hoechst). Scale bars, 50 µm (left panel) and 10 µm (enlarged panel on the right), respectively. (**D**) Percentage of number of mCherry^{+} cells in Fos^{+} neurons in *Tac2*-Cre mice receiving CNO injection (0.5 mg/kg, i.p.). Four series of representative images from N = 3 mice. (**E**) Schematic showing strategy for resident-intruder test in *Tac2*-Cre mice injected with DREADDs vectors. (**F**) Representative raster plots showing mouse attack (red bar) or exploring behavior (gray bar) during resident-intruder assay. Time scale, 1 min. (**G-I**) Quantification of Latency to attacks (**G**), Number of attacks (**H**) and Duration of attacks (**I**). N = 10 in *Tac2*^{hM3Dq} group and N = 7 in *Tac2*^{mCherry} group. Data represent mean ± S.E.M. Significance was calculated by means of unpaired *t*-test. ** $P < 0.01$, *** $P < 0.001$, **** $P < 0.0001$. Schematics (panel A and E) are created with BioRender.com.

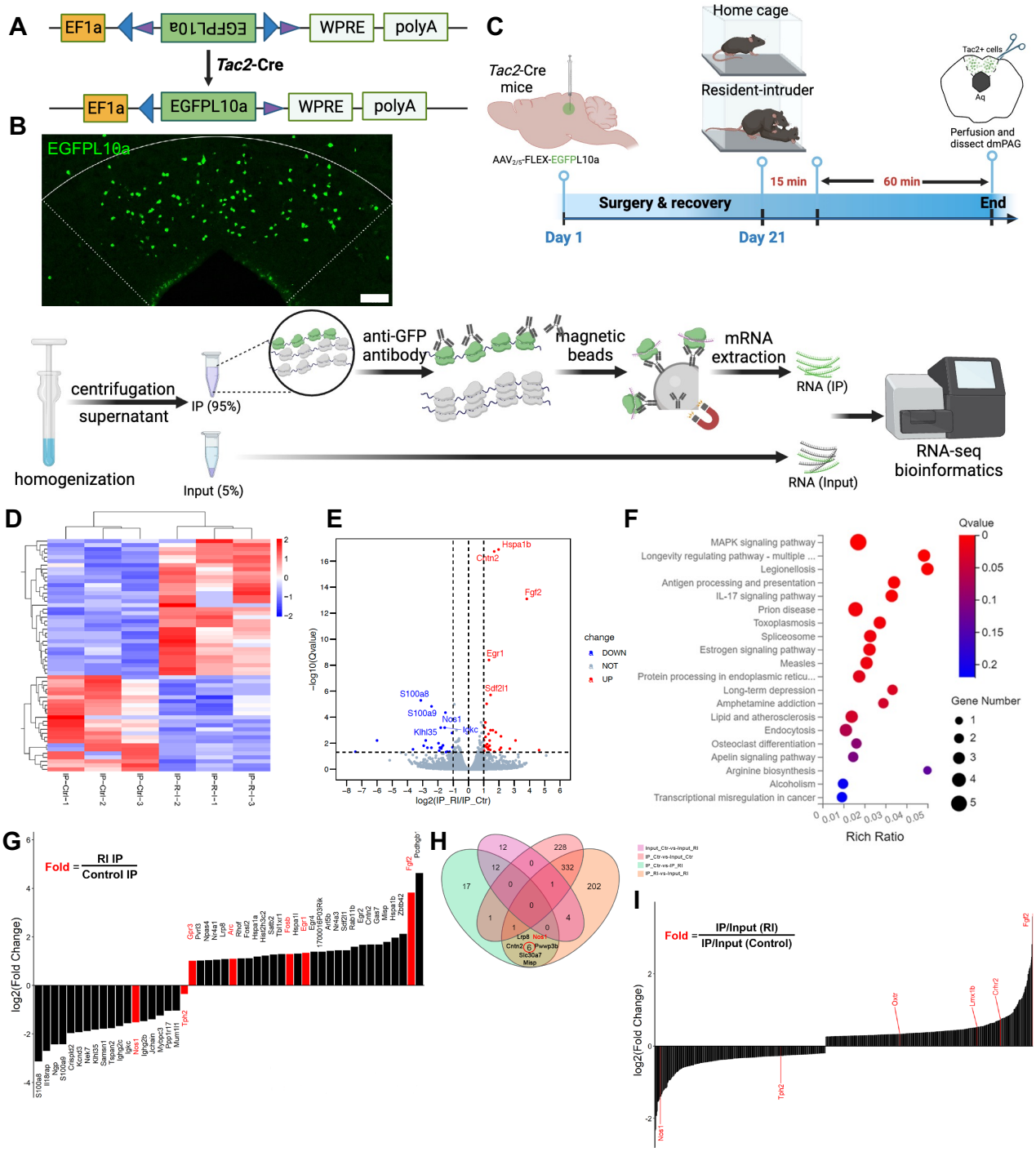

Figure 5. TRAP-seq reveals transcriptional alterations following fighting behaviors

(**A**) Vector information for expressing a Cre-dependent TRAP vector in *Tac2*-Cre mice. (**B**) Representative fluorescent images of EGFPL10a protein (green) in dmPAG. Scale bar, 100 µm. (**C**) Schematic showing strategy for TRAP-seq in *Tac2*-Cre mice injected with AAV-FLEX-EGFPL10a in the dmPAG and subjected to resident-intruder (RI) test or home cage (control). (**D**) Heatmap showing DEGs of the IP samples. $|\log_2 FC|>1$, adjusted q value<0.05. (**E**) Volcano plot showing DEGs of the IP samples. (**F**) KEGG enrichment analysis showing top 20 most enriched pathways affected by RI when compared to the control group. (**G**) Fold-change analysis showing $\log_2(FC)$ value of RI-IP to Control-IP samples. Red genes are immediate-early genes (*Gpr3*, *Arc*, *Fosb*, *Egr1*, *Fgf2*) or genes enlisted for subsequent validation experiment (*Nos1* and *Trph2*). (**H**) Venna plot showing DEG genes in each comparison (input_ctr vs Input_RI, IP_ctr vs input_Ctr, IP_ctr vs IP_RI, and IP_RI vs input_RI). Six genes were identified as common DEGs by comparisons of IP_ctr vs IP_RI and IP_RI vs input_RI. (**I**) A secondary analysis of enrichment score, based on normalizing IR/Input (RI) to IR/Input (Control). Note that *Nos1*, *Tph2*, *Oxtr*, *Lmx1b*, *Crhr2*, and *Fgf2* (labeled in red on the left) were listed among the most enriched genes that were related to the 5-HT system. Schematics (panel A and C) are created with BioRender.com.

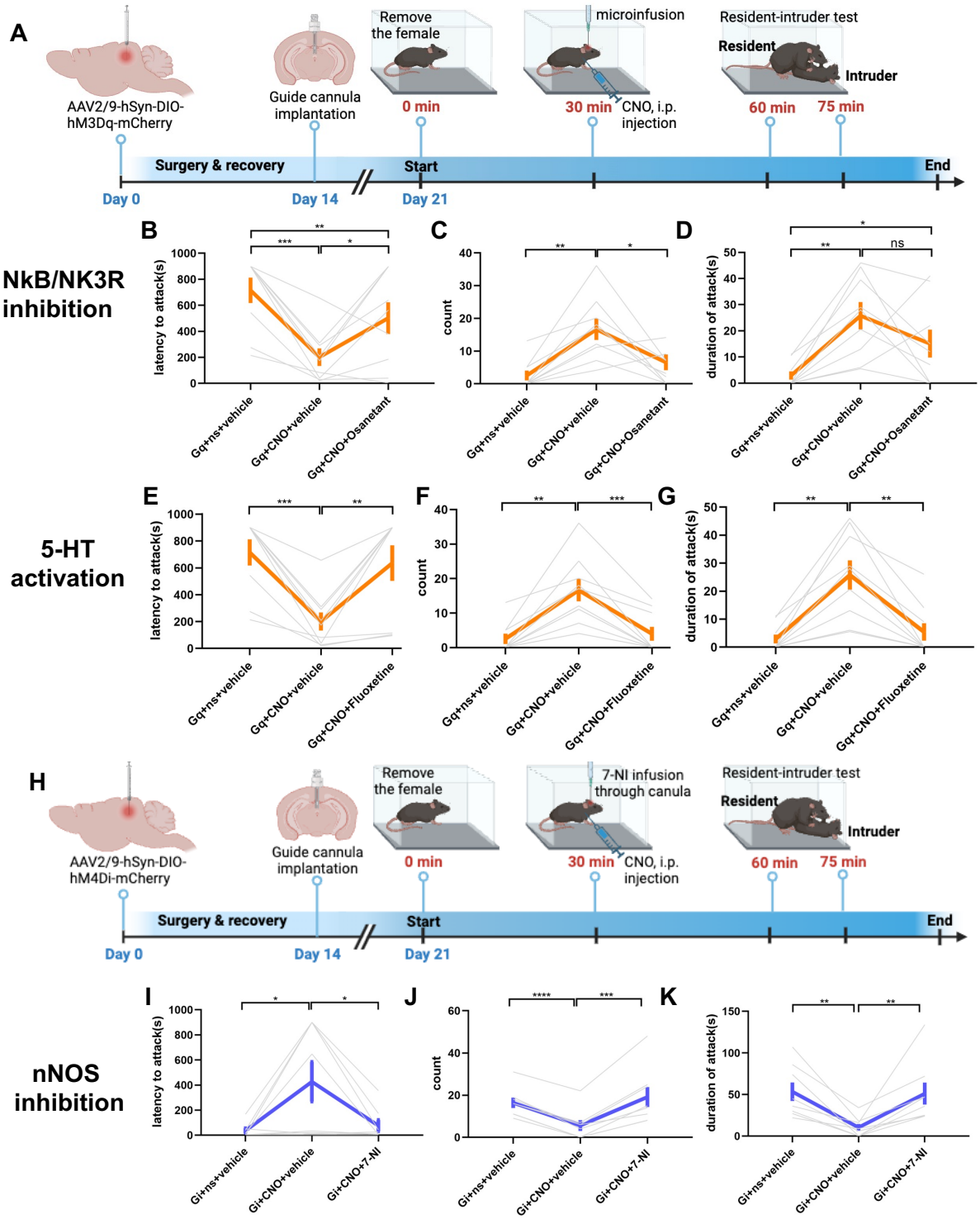

<u>Figure 6</u>. Pharmacological validation of molecular targets identified by TRAP-seq.

(**A**) Schematic showing strategy for inhibition of NkB/NK3R pathway with Osanetant or activation of the 5-HT system with Fluoxetine using microinfusion in dmPAG of *Tac2*-Cre mice injected with excitatory DREADDs vectors and subjected to the resident-intruder test. (**B-D**) Quantification of latency to attacks (**B**), number of attacks (**C**) and duration of attacks (**D**) in Tac2^{hM3dq} mice injected with Osanetant. N = 9 in each group in panel (**B-D**). (**E-G**) Quantification of latency to attacks (**E**), number of attacks (**F**) and duration of attacks (**G**) in Tac2^{hM3dq} mice injected with Fluoxetine. N = 9 in each group in panel (**E-G**). (**H**) Schematic showing strategy for inhibition of nNOS system with 7-NI microinfusion in dmPAG of *Tac2*-Cre mice injected with inhibitory DREADDs vectors and subjected to the resident-intruder test. (**I-K**) Quantification of latency to attacks (**I**), number of attacks (**J**) and duration of attacks (**K**) in Tac2^{hM4di} mice injected with 7-NI. N = 9 in each group in panel (**I-K**). Data represent mean ± S.E.M. Significance was calculated by means of unpaired *t*-test. * $P < 0.05$, ** $P < 0.01$, *** $P < 0.001$, **** $P < 0.0001$. Schematics (panel A and H) are created with BioRender.com.

EXPERIMENTAL MODEL AND STUDY PARTICIPANT DETAILS

Animals

Adult (8-10 weeks) *Tac2*-Cre (Jackson, strain name B6.129-Tac2tm1.1(cre)Qima/J, stock number 018938), Ai9-tdTomato reporter mice (Jackson, stain name B6.Cg-Gt(ROSA)26Sortm9(CAG-tdTomato)Hze/J, stock number 7909), and Wild-type (WT) mice were used in this study. *Tac2*-Cre mice were kindly provided by Prof. Minmin Luo at the Chinese Institute for Brain Research, Beijing, China. Ai9 tdTomato reporter mice were kindly provided by Prof. Jian-Zhi Wang and Prof. Yunyun Han at Huazhong University of Science and Technology, Wuhan, China. All the mice were on a C57BL/6J background and were under a 12h/12h light-dark cycle with food and water provided *ad libitum*. Mice that were used for resident-intruder test were separately housed in a cage with a female spouse for at least one week before the start of the test, whereas other mice were all group housed (maximum four mice per cage). All procedures were approved by institutional guidelines and the Animal Care and Use Committee (Huazhong University of Science and Technology, Wuhan, China) of the university's animal core facility.

METHOD DETAILS

Viral vectors

$AAV_{2/9}$-hSyn-DIO-mCherry, $AAV_{2/9}$-EF1a-DIO-mCherry-P2A-TVA, $AAV_{2/9}$-EF1a-DIO-RVG, $AAV_{2/5}$-EF1a-DIO-DTA were prepared by BrainVTA Co., Ltd (Wuhan, China). $AAV_{2/9}$-hSyn-GCaMP6m, $AAV_{2/9}$-hSyn-DIO-GCaMP6m, $AAV_{2/9}$-hSyn-DIO-hM3Dq-mCherry, and $AAV_{2/9}$-hSyn-DIO-hM4Di-mCherry were prepared by Shanghai Taitool Bioscience Co., Ltd (Shanghai, China). $AAV_{2/5}$-FLEX-EGFPL10a was purchased from Addgene. The final titers of these viral vectors were estimated to be 10^{13} genome copies per milliliter. All viral vectors were subpackaged and stored at -80℃ until use to avoid repeated freezing and thawing.

Stereotaxic Surgeries and Viral injections

All stereotaxic surgeries were performed under general anesthesia using a stereotaxic apparatus (Stoelting, Wood Dale, USA). Mice were intraperitoneally anaesthetized with chloral hydrate (350 mg/kg) and xylazine (10 mg/kg) before fixed at a mouse adaptor (RWD life science, Shenzhen). During the surgery period, anesthetics were added, when necessary, by subcutaneous injection according to the state of anesthesia. In addition, a heating pad was also attached to the mouse adaptor to maintain a stable body temperature. After fixation on the adaptor, mice were eye-protected with ointment and transferred to a stereotactic apparatus. After the skull was exposed and leveled on the stereotactic, drilling was performed, followed by an injection of concentrated viral vector into the dmPAG (AP: -4.48 mm, ML: -0.03 mm, DV: -2.0 mm) using calibrated glass microelectrodes connected to an infusion pump (SYS-Micro4, WPI, UK) at a speed of 30 nl/min. The coordinates used above, especially the DV, were slightly adjusted according to the body weight of mice. The injection needle was held in position for 10 minutes and then was withdrew, Subsequently, the incision was closed with a suture and a tissue adhesive (Vetbond, 3M, USA). The animal was kept on a heating pad until fully recovered from anesthesia. Injection sites were confirmed by preparing coronal sections (20 μm) of injection sites with immunofluorescence staining.

In vivo fiber photometry recording

We first injected an AAV vector encoding GCamP6m (AAV-hSyn-DIO-GCamp6m, 2.4×10^{13} vg/ml, 200nl) into the dmPAG. Two weeks later, a unilateral implantation of a chronically implanted optical fiber (200 μm, NA = 0.37; Inper Inc) was performed on mice, which was about 200 μm above the dmPAG (AP: -4.48 mm, ML: -0.03 mm, DV: -1.8 mm) and fixed to the mouse skull with screws and dental cement. Mice were allowed for recovery at least 7 days after optical fiber implantation until then the resident-intruder test was performed (see below). During the 15min-test, behavioral performance was videotaped and calcium activity of dmPAG neurons, which was reflected by fluorescence change of GCaMP6m, was recorded. We performed baseline correction, motion correction and signaling filtering using Inper Data Process Software (Inper Inc, China) to process the raw data from fiber photometry recording. GraphPad Prism (v8, GraphPad Inc.) and MATLAB (R2017a) were used for data processing. Changes of fluorescence value, i.e., $\Delta F/F$, was calculated as $(F_t-F_0)/F_0$, in which the F_0 was the average baseline value of calcium signal prior to attack, and F_t was the calcium signal value from 6 s to 2 s before attack, that is, the average value of calcium signal from -6 s to -2 s when attack was launched. Finally, optical fiber placements were verified by preparing immunofluorescence staining of coronal sections (20 μm) covering the implantation sites after finishing all the recording.

Rabies tracing

The rabies viral tracing was built on Cre-dependent co-expression of avian receptor TVA and rabies glycoprotein G (RVG) on principle neurons through co-injecting helper viruses (AAV-EF1a-DIO-mCherry-P2A-TVA and AAV-EF1a-DIO-RVG) into the region of interest (Wall *et al.*, 2010). First, these two helper viruses were injected into dmPAG (AP: -4.48 mm, ML: -0.03 mm, DV: -2.0 mm) of *Tac2*-cre mice at day 1. Then, at day 21, a genetically modified rabies virus pseudotyped with an avian envelop protein (RV-ENVA-ΔG-EGFP) was delivered to the same coordinates. Seven days after RV injection mice were perfused and brain slices was obtained for further imaging and analysis.

Behavioral Assays

All mice were transferred to the testing room for the habituation of the environments at least 3 hrs prior to all tests. When the entire testing trial of each mouse finished, all behavioral apparatus were cleaned with 75% ethanol to eliminate the odor left by the previous mice. All behavioral tests were performed during the dark cycle of the mice.

Open-field test

Open-field test was performed as previously reported with minor modifications (Li et al., 2023; Qi et al., 2022; Zhang et al., 2019). Briefly, a white open-field box (50 cm × 50 cm × 50 cm) made of PVC materials was used. During the test, mice were placed gently in the center of the open arena as a starting position and were allowed to explore freely for 10 min. Data were recorded and analyzed using SuperMaze software (Shanghai Xinruan, Shanghai). Total distance travelled in the open filed area, time spent in the central zone and total numbers of entries into the central zone were analyzed to evaluate spontaneous activity in these mice.

Elevated-plus maze test

Elevated-plus maze (EPM) test was performed as previously reported with minor modifications (Li *et al.*, 2023; Qi *et al.*, 2022; Zhang *et al.*, 2019). Briefly, we used an EPM apparatus placed 62 cm in height from the ground.

This apparatus was made of two open arms (75 cm × 5 cm) and two closed arms (75 cm × 5 cm × 15 cm) (Shanghai Xinruan, Shanghai). To start the test, mice were placed gently in the center area of the maze, with the mice facing to the open arm. Mice behaviors in the maze were recorded for 8 minutes using SuperMaze software (Shanghai Xinruan, Shanghai). Time spent in open or closed arms and numbers of total entries into openor closed arms were analyzed.

Three-chamber social interaction (SI) test

The three-chamber social interaction test was conducted in a rectangular Plexiglass box (60 cm × 40 cm × 22 cm) as reported previously (Li *et al.*, 2023; Qin et al., 2018; Rein et al., 2020). The testing box was separated into 3 equal chambers by 2 clear Plexiglass walls, each contains an entryway that mice can move with free access. A wire cage (5 cm in diameter and 10 cm in height) was placed in the center of the 2 side chambers. To start each test, mouse was placed in the middle chamber as the starting point. For Session #1 (habituation), empty wire cage was placed in the two side chambers as noted above. Mice were allowed to explore the apparatus freely for 10 min. During Session #2 (sociability test), a stranger social mouse, whose species and sex were the same as the testing mouse, was placed inside one of the wire cages at one side chamber, then were allowed to explore the apparatus freely for 10 min. During Session #3 (social novelty test), a new stranger social mouse, whose species and sex were the same as the testing mouse but coming from a different cage as the previously caged mouse, was placed inside another wire cage that was empty during Session #2. The testing mouse was allowed to explore the apparatus freely for another 10 min. There are a 5-minute inter-session interval after each session. Data were recorded, retrieved and analyzed by using SuperMaze software (Shanghai Xinruan, Shanghai). Social preference score was calculated as $(T_S-T_{NS})/(T_S+T_{NS})$, in which T_S or T_{NS} represented the time that a testing mouse spent in the social area or non-social area, respectively.

Resident-intruder test

Resident-intruder test, a classical paradigm to test aggressive behaviors in mice, was performed as reported previously (Koolhaas et al., 2013). The resident-intruder test varies depending on different research focus and purpose of experiment (Jager *et al.*, 2018). Here, mice subjected to resident-intruder test ("resident") were housed with a female companion for at least 7 days before the test, which increased their sense of territory. During this period, the bedding material was kept clean but the same. Previously, research suggested that chronic social isolation broadly upregulated Tac2/NkB signaling across the brain areas (Zelikowsky *et al.*, 2018), we did not choose the commonly used paradigm for resident-intruder test, in which the testing mice are single-housed prior to the test to increase levels of aggression. One hour before the test, the female companion mouse was removed from the cage, and a stranger C57/bl6 male mouse ("intruder"), which was slightly smaller in body size than the resident, was introduced into the cage and allowed to interact for 15 minutes freely. During the test, videos were recorded (Shanghai Xinruan, Shanghai), and latency to attack, numbers of attack episode, and duration of attack were analyzed using Adobe Premiere Pro CC 2018 and GraphPad Prism 8.0.

Chemogenetic modulation of dmPAG^{Tac2} neurons

Chemogenetic manipulation experiment was performed based on previous reports (Chen et al., 2020; Falkner *et al.*, 2020; Hashikawa *et al.*, 2017; Karigo et al., 2021; Zha *et al.*, 2020). For chemogenetic activation of

dmPAG^{Tac2} neurons with hM3Dq (Gq) vectors, *Tac2*^{hM3Dq} mice received stereotaxic injection of AAV2-hSyn-DIO-hM3Dq-mChery (1.22×10^{13} vg/ml, 200 nl) into the dmPAG. Control mice (*Tac2*^{mCherry}) were injected with AAV2-hSyn-DIO-mChery (5×10^{12} vg/ml, 500nl). Twenty-one days after injections, mice were tested for aggression for 3 consecutive days. Mice were intraperitoneally injected with either 0.5 mg/kg CNO (Sigma, C0832) or equivalent amount of saline once their levels of aggression was stabilized. 30 minutes afterwards, these mice were tested for resident-intruder (as described above) to evaluate their levels of aggression. To verify the efficacy of CNO administration, *Tac2*-cre mice were injected with Gq vectors were given 0.5 mg/kg CNO i.p. at the natural state (i.e., durign home-cage housing state). 120 minutes later, these mice were sacrificed and perfused to collect brain tissues for subsequent c-Fos immunofluorescence.

For chemogenetic inhibition of dmPAG^{Tac2} neurons with hM4Di (Gi) vectors, *Tac2*^{hM4Di} mice received AAV2-hSyn-DIO-hM4Di-mChery (1.77×10^{13} vg/ml, 150 nl) injection stereotactically at dmPAG. Control mice (*Tac2*^{mCherry}) were injected with AAV2-hSyn-DIO-mChery (5×10^{12} vg/ml, 500 nl). Twenty-one days after injections, mice were tested for aggression for 3 consecutive days. Mice were i.p. injected with either 1.0 mg/kg CNO (Sigma, C0832) or the equivalent amount of saline once their levels of aggression was stabilized. 30 minutes afterwards, these mice were tested for resident-intruder to evaluate their levels of aggression.

Genetic ablation of dmPAG^{Tac2} neurons

Tac2-Cre mice were tested for aggression before receiving virus injection for genetic ablation. To genetically ablate *Tac2*-expressing cells in the dmPAG, we specifically expressed diphtheria toxin (DTA) in dmPAG^{Tac2} neurons by injecting AAV-hSyn-DIO-DTA-mCherry (5.89×10^{12} vg/ml, 450nl) into the dmPAG of *Tac2*-Cre mice. Control *Tac2*-Cre mice were injected at the same region with an equal volume the control viral vector (AAV-hSyn-DIO-mCherry) which does not contain the DTA construct. Twenty-one days following viral injection, mice were subjected for resident-intruder test again.

Immunofluorescence

Immunofluorescent staining was performed as reported previously (Takeda et al., 2022; Xu et al., 2019). Briefly, mice were perfused with ice-cold 0.9% normal saline, followed by perfusion with ice-code 4% paraformaldehyde. After perfusion, whole brains were carefully from the skull and fixed in 4% paraformaldehyde for 6 hours at 4℃ for post-fixation and then transferred to 20% and 30% sucrose solution for gradient dehydration.

To explore and verify expression of Tac2 protein across the whole brain, brains from *Tac2*-Cre/Ai9-tdT double heterogeneous mice were obtained (same as the above immunofluorescent procedure). After gradient dehydration, coronal sections were prepared from frozen brain tissues via Leica 1860 vibratome at a thickness of 30 μm. Brain slices were rinsed in PBS 3 times (5 min each) and then were stained with Hoechst (1:1000, #33342, Sigma-Aldrich) for 10 min. These slices were rinsed in PBS 3 times again (5 min each) and were cover-slipped with fluorescent mounting medium (Beyotime Shanghai, China) and proceeded with imaging immediately.

To confirm immunofluorescent expression and verify the viral injection site, brains of mice that were subjected to stereotaxic surgeries were obtained (same as the above immunofluorescent procedure). Coronal frozen sections of the PAG region, which consisted of about 90 series slices, were prepared at a thickness of 30 μm. The staining

procedure is the same as above. For rabies tracing experiment, brains of mice that were subjected to RV-assisted tracing were obtained. Coronal frozen sections of the whole-brain areas were prepared at a thickness of 20 μm. Then, the sectioned brain slices were rinsed in PBS 3 times (5 min each) and then stained with Hoechst for 10 min. These slices were rinsed in PBS 3 times again (5 min each) and were cover-slipped with fluorescent mounting medium. After staining, slices were proceeded with imaging immediately.

For c-Fos staining experiment, we followed a previous report (Park et al., 2018). brains of mice that were subjected to resident-intruder test were sacrificed 90 minutes after the test, or sacrificed 120 minutes after receiving CNO administration. Coronal frozen sections of the whole-brain areas (for c-Fos mapping) or the PAG area (for CNO administration) were prepared at a thickness of 20 μm. Subsequently, the brain slices were permeabilized with 0.3% Triton X-100 in PBS for 10 min and blocked with 5% bovine serum albumin (BSA) in PBS for 1 hr. The brain slices were then incubated with primary antibodies (1:800, rabbit monoclonal anti-cFos antibody, #2250S, Cell Signaling) at 4 °C overnight. Following incubation with primary antibodies, brain slices were rinsed 3 times in PBS (5 min each) and then were incubated in fluorochrome-conjugated secondary antibody (1:200, Dylight^{488}-conjugated goat anti-rabbit Abbkine; 1:200, AF^{488}-conjugated goat anti–rabbit IgG Jackson ImmunoResearch) for 1 h at room temperature in dark. These slices were then rinsed for 3 times in PBS (5 min each) and then stained nuclei with Hoechst (1:1000, #33342, Sigma-Aldrich) for 10 min. Afterwards, the slices were rinsed for 3 times in PBS again (5 min each), cover-slipped with fluorescent mounting medium and stored in 4 °C prior to confocal imaging.

Translating Ribosome Affinity Purification (TRAP) and RNA Sequencing

Affinity purification of translating ribosomes was performed as described (Heiman *et al.*, 2014) with minor modifications. Briefly, *Tac2*-Cre mice were subjected to stereotaxic viral injection of AAV-EF1a-FLEX-EGFPL10a (7×10^{12} vg/ml, 400 nl) in the dmPAG. Three weeks later, brain areas containing dmPAG were rapidly dissected (individual dmPAG were pooled from 6-7 mice per sample; thus, each group there were 3 replicates) at 4 °C (cold room) and were immediately transferred into ice-cold dissection buffer for tissue wash to remove blood. These samples were then transferred to a pre-chilled homogenizer on ice that contains tissue-lysis buffer (20 mM HEPES, pH 7.4, 10 mM $MgCl_2$, 150 mM KCl, 0.5 mM DTT, 100 mg/ml cycloheximide, 10 μl/ml RNasin and Superasin). We used a pre-cooled Dounce and a loose pestle to homogenize the tissue for 20 times, a tight pestle for 20 times. Homogenates were then centrifuged at 2,000g, 10 min, at 4 °C, to pellet large cell debris. NP-40 (Beyotime Biotechnology, Shanghai) and 1,2-diheptanoyl-sn-glycero-3-phosphocholine (Avanti Polar Lipids, AL) were added to the supernatant at final concentrations of 1% and 30 mM, respectively. After incubation on ice for 5 min, the lysates were centrifuged for 10 min at 20,000g to pellet insoluble materials. A small amount of supernatant (about 5%) was collected in separated centrifuge tubes, which representing "*Input*" fraction. GFP antibodies (Proteintech, 5ug) were added into the remaining supernatant for an end-over-end incubation (4 hrs, at 4 °C) on a rotator. Protein A+G magnetic beads (Beyotime Biotechnology) were prepared during the incubation. The cleaned beads were then added to the tissue homogenates when the incubation was finished. The tissue homogenates were allowed to continue the end-over-end incubation for another 16-18 hrs at 4°C. The next day, when the incubation was finished, the beads were resuspended with high-salt buffer (20 mM HEPES KOH, pH 7.3, 350 mM KCl, 10 mM $MgCl_2$, and 1% NP-40, 0.5 mM DTT, 100 μg/ml cycloheximide

and Rnasin) at least 4 times. After the last cleaning of the beads, pre-cooled centrifuge tubes were placed on the magnet holder for at least 1 min, and all remaining cleaning fluid was carefully removed. Afterwards, RLT buffer (Qiagen Kit 74004, DTT added) were added to the tubes, and these tubes were removed from the magnet holder and vortexed for 30s at room temperature. Subsequently, the tubes were placed on the magnet holder for at least 1 min at room temperature. Then, the RLT buffer that containing RNAs was transferred to new enzyme-free centrifuge tubes, which representing "*IP*" fraction. To isolate RNAs from "*Input*" fractions, RLT buffer was added to the *Input* samples and vortexed thoroughly. RNA extraction was performed side-by-side with the *IP* samples according to the instructions of RNA isolation kits. Finally, extracted RNAs or RLT lysate containing RNAs was sent to Shanghai Bohao Biotechnology for RNA quality inspection and subsequent library construction and mRNA constant sequencing analysis.

Intra-dmPAG drug delivery for pharmacological validation

Pharmacological validation experiments were based on previous reports with minor modifications (Andero *et al.*, 2014; Artur de la Villarmois et al., 2020; Carlini et al., 2007; Lee et al., 1992; Ota et al., 2010; Shen et al., 2014; Zelikowsky *et al.*, 2018). First, we performed stereotaxic injection of AAV2-hSyn-DIO-hM3Dq-mCherry or AAV2-hSyn-DIO-hM4Di-mCherry vectors into the dmPAG of *Tac2*-Cre mice. Two weeks later, these mice were implanted with a guide cannula at dmPAG (AP: -4.48 mm, ML: -0.03 mm). The depth of the injection catheter base was determined according to the final injection site in the target brain area and the depth of the matching injection tube. For instance, the injection site of the dmPAG of 25 g mice in this study was -2.0 mm. If the implantation depth of the injection catheter base was -1.40 mm, an injection tube of G1 = 0.6 mm was used. If the implantation depth of the drug delivery catheter base is -1.50 mm, an injection tube of G1 = 0.5 mm was then used. The implantation depth of the drug delivery catheter in each mouse is recorded so that the corresponding length of the injection tube can be used in the subsequent drug administration. The catheter cap should be inserted into the implanted drug delivery catheter to maintain the patency of the catheter, to prevent thrombosis, and to reduce intracranial infection when the drug is not injected daily.

Seven days after cannula implantation, we delivered selected pharmacological agents into dmPAG. These agents include Nk3R antagonist osanetant (Axon Medchem, 500 ng/400nl), nNOS inhibitor 7-Nitroindazole (7-NI, 2μg/500nl), Fluoxetine (MCE, 6 μg/500nl), or vehicle (normal saline with Tween 20 for osanetant, saline with DMSO for 7-NI or Fluoxetine. Injection volumes were adjusted to the same level of corresponding experimental groups. Of note, osanetant and fluoxetine were chosen to reverse the effects of chemogenetic activation of $dmPAG^{Tac2}$ neurons, whereas 7-NI was chosen to rescue the effects of chemogenetic inhibition of $dmPAG^{Tac2}$ neurons.

Prior to behavioral tests following for intra-dmPAG, the guide cannula (RWD Life Science, Shenzhen, China) was removed from the testing mice and replaced with injection cannula, which protruded 0.5mm-0.7mm from the tip of the guide cannula according to the implantation sites of the guide base. The Injection cannula were attached to a 10-ml Hamilton syringe with PE tubing. Testing drugs were delivered through the injection pump at a rate of 0.25 μl/min to inject a total volume of 500 nl of drug. When the drug delivery was finished, the injection cannula was held in place for another 3 minutes to allow fully diffusing the drugs into the dmPAG and

to prevent the backflow of the testing drugs while the needle pulled out. Afterwards, the injection tube was carefully and slowly pulled out, and the remaining drugs in the PE tube were continued to push out to verify the patency of the needle. After intracranial injection, CNO was intraperitoneally administered immediately. The guide cannula was sterilized, and then inserted into the guide base. Behavioral tests were performed around 30 min after the CNO administration.

QUANTIFICATION AND STATISTICAL ANALYSIS

The data obtained were processed and analyzed by various softwares when necessary (Excel, GraphPad, ImageJ). Statistical analyses were mainly involved unpaired *t*-test, paired *t*-test, one-way analysis of variance (one-way ANOVA), two-way ANOVA for the homogeneity of variance of data with normal distribution. Turkey test was used for multi-comparisons between specific groups following ANOVA. Data are expressed as mean ± standard error (mean ± s.e.m.). Statistical difference was indicated with * $P < 0.05$, ** $P < 0.01$, *** $P < 0.001$, **** $P < 0.0001$. Specifically, one-way ANOVA analysis was used to compare fluorescent staining in different brain region, paired *t*-test was used to compare behavioral data of chemogenetic manipulation and intra-dmPAG drug microinfusion, unpaired *t*-test was used to compare the behavioral results of WT mice and *Tac2*-Cre mice in open-field test, elevated plus maze test, and rotarod test, and two-way ANOVA was used to analyze behavioral data of three-chamber social interaction test. Results of ablation of $dmPAG^{Tac2}$ neurons was analyzed by unpaired and paired *t*-tests. In addition, behavior data from resident-intruder test were collected by Xinsoft XR-XZ301 video acquisition and analysis system, and video analysis and statistics were performed by Premiere Pro CC 2018. A double-blind analysis of these videos was performed by at least two people not aware of the group information, and ultimately the mean of the two statistically collected data was taken for further statistical analysis.

References

Andero, R., Dias, B.G., and Ressler, K.J. (2014). A role for Tac2, NkB, and Nk3 receptor in normal and dysregulated fear memory consolidation. Neuron *83*, 444-454. 10.1016/j.neuron.2014.05.028.

Anderson, C.A., and Bushman, B.J. (2002). Human aggression. Annu Rev Psychol *53*, 27-51. 10.1146/annurev.psych.53.100901.135231.

Artur de la Villarmois, E., Gabach, L.A., Bianconi, S., Poretti, M.B., Occhieppo, V., Schioth, H.B., Carlini, V.P., and Perez, M.F. (2020). Pharmacological NOS-1 Inhibition Within the Hippocampus Prevented Expression of Cocaine Sensitization: Correlation with Reduced Synaptic Transmission. Mol Neurobiol *57*, 450-460. 10.1007/s12035-019-01725-3.

Bianchi, M., Moser, C., Lazzarini, C., Vecchiato, E., and Crespi, F. (2002). Forced swimming test and fluoxetine treatment: in vivo evidence that peripheral 5-HT in rat platelet-rich plasma mirrors cerebral extracellular 5-HT levels, whilst 5-HT in isolated platelets mirrors neuronal 5-HT changes. Exp Brain Res *143*, 191-197. 10.1007/s00221-001-0979-3.

Bindi, R.P., Guimaraes, C.C., de Oliveira, A.R., Melleu, F.F., de Lima, M.A.X., Baldo, M.V.C., Motta, S.C., and Canteras, N.S. (2023). Anatomical and functional study of the cuneiform nucleus: A critical site to organize innate defensive behaviors. Ann N Y Acad Sci *1521*, 79-95. 10.1111/nyas.14954.

Blanchard, R.J., Wall, P.M., and Blanchard, D.C. (2003). Problems in the study of rodent aggression. Horm Behav *44*, 161-170. 10.1016/s0018-506x(03)00127-2.

Borelli, K.G., Ferreira-Netto, C., and Brandao, M.L. (2006). Distribution of Fos immunoreactivity in the rat brain after freezing or escape elicited by inhibition of glutamic acid decarboxylase or antagonism of GABA-A receptors in the inferior colliculus. Behav Brain Res *170*, 84-93. 10.1016/j.bbr.2006.02.015.

Brunner, H.G., Nelen, M., Breakefield, X.O., Ropers, H.H., and van Oost, B.A. (1993). Abnormal behavior associated with a point mutation in the structural gene for monoamine oxidase A. Science *262*, 578-580. 10.1126/science.8211186.

Canteras, N.S., and Goto, M. (1999). Fos-like immunoreactivity in the periaqueductal gray of rats exposed to a natural predator. Neuroreport *10*, 413-418. 10.1097/00001756-199902050-00037.

Carey, T.S., Sanders, G.D., Viswanathan, M., Trikalinos, T.A., Kato, E., and Chang, S. (2012). In Framework for Considering Study Designs for Future Research Needs.

Carlini, V.P., Gaydou, R.C., Schioth, H.B., and de Barioglio, S.R. (2007). Selective serotonin reuptake inhibitor (fluoxetine) decreases the effects of ghrelin on memory retention and food intake. Regul Pept *140*, 65-73. 10.1016/j.regpep.2006.11.012.

Carreno Gutierrez, H., O'Leary, A., Freudenberg, F., Fedele, G., Wilkinson, R., Markham, E., van Eeden, F., Reif, A., and Norton, W.H.J. (2020). Nitric oxide interacts with monoamine oxidase to modulate aggression and anxiety-like behaviour. Eur Neuropsychopharmacol *30*, 30-43. 10.1016/j.euroneuro.2017.09.004.

Carrive, P. (1993). The periaqueductal gray and defensive behavior: functional representation and neuronal organization. Behav Brain Res *58*, 27-47. 10.1016/0166-4328(93)90088-8.

Caruso, R., Antenora, F., Riba, M., Belvederi Murri, M., Biancosino, B., Zerbinati, L., and Grassi, L. (2021). Aggressive Behavior and Psychiatric Inpatients: a Narrative Review of the Literature with a Focus on the European Experience. Curr Psychiatry Rep *23*, 29. 10.1007/s11920-021-01233-z.

Cases, O., Seif, I., Grimsby, J., Gaspar, P., Chen, K., Pournin, S., Muller, U., Aguet, M., Babinet, C., Shih, J.C., and et al. (1995). Aggressive behavior and altered amounts of brain serotonin and norepinephrine in mice lacking MAOA. Science *268*, 1763-1766. 10.1126/science.7792602.

Chen, A.X., Yan, J.J., Zhang, W., Wang, L., Yu, Z.X., Ding, X.J., Wang, D.Y., Zhang, M., Zhang, Y.L., Song, N., et al. (2020). Specific Hypothalamic Neurons Required for Sensing Conspecific Male Cues Relevant to Inter-male Aggression. Neuron *108*, 763-774 e766. 10.1016/j.neuron.2020.08.025.

Chen, Z., Chen, X., Liu, M., Liu, S., Yu, S., and Ma, L. (2018). Magnetic Resonance Image Texture Analysis of the Periaqueductal Gray Matter in Episodic Migraine Patients without T2-Visible Lesions. Korean J Radiol *19*, 85-92. 10.3348/kjr.2018.19.1.85.

Chiavegatto, S., Dawson, V.L., Mamounas, L.A., Koliatsos, V.E., Dawson, T.M., and Nelson, R.J. (2001). Brain serotonin dysfunction accounts for aggression in male mice lacking neuronal nitric oxide synthase. Proc Natl Acad Sci U S A *98*, 1277-1281. 10.1073/pnas.98.3.1277.

Coccaro, E.F., Fanning, J.R., Phan, K.L., and Lee, R. (2015). Serotonin and impulsive aggression. CNS Spectr *20*, 295-302. 10.1017/S1092852915000310.

de Jong, J.W., Afjei, S.A., Pollak Dorocic, I., Peck, J.R., Liu, C., Kim, C.K., Tian, L., Deisseroth, K., and Lammel, S. (2019). A Neural Circuit Mechanism for Encoding Aversive Stimuli in the Mesolimbic Dopamine System. Neuron *101*, 133-151 e137. 10.1016/j.neuron.2018.11.005.

Demas, G.E., Eliasson, M.J., Dawson, T.M., Dawson, V.L., Kriegsfeld, L.J., Nelson, R.J., and Snyder, S.H. (1997). Inhibition of neuronal nitric oxide synthase increases aggressive behavior in mice. Mol Med *3*, 610-616.

Deng, H., Xiao, X., and Wang, Z. (2016). Periaqueductal Gray Neuronal Activities Underlie Different Aspects of Defensive Behaviors. J Neurosci *36*, 7580-7588. 10.1523/JNEUROSCI.4425-15.2016.

Dielenberg, R.A., Hunt, G.E., and McGregor, I.S. (2001). "When a rat smells a cat": the distribution of Fos immunoreactivity in rat brain following exposure to a predatory odor. Neuroscience *104*, 1085-1097. 10.1016/s0306-4522(01)00150-6.

Dombret, C., Naule, L., Trouillet, A.C., Parmentier, C., Hardin-Pouzet, H., and Mhaouty-Kodja, S. (2020). Effects of neural estrogen receptor beta deletion on social and mood-related behaviors and underlying mechanisms in male mice. Sci Rep *10*, 6242. 10.1038/s41598-020-63427-4.

Falkner, A.L., Wei, D., Song, A., Watsek, L.W., Chen, I., Chen, P., Feng, J.E., and Lin, D. (2020). Hierarchical Representations of Aggression in a Hypothalamic-Midbrain Circuit. Neuron *106*, 637-648 e636. 10.1016/j.neuron.2020.02.014.

Fields, R.D. (2019). THE ROOTS OF HUMAN AGGRESSION: Experiments in humans and animals have started to identify how violent behaviors begin in the brain. Sci Am *320*, 65-71.

Florido, A., Velasco, E.R., Soto-Faguas, C.M., Gomez-Gomez, A., Perez-Caballero, L., Molina, P., Nadal, R., Pozo, O.J., Saura, C.A., and Andero, R. (2021). Sex differences in fear memory consolidation via Tac2 signaling in mice. Nat Commun *12*, 2496. 10.1038/s41467-021-22911-9.

Forstermann, U., and Sessa, W.C. (2012). Nitric oxide synthases: regulation and function. Eur Heart J *33*, 829-837, 837a-837d. 10.1093/eurheartj/ehr304.

Franklin, T.B. (2019). Recent Advancements Surrounding the Role of the Periaqueductal Gray in Predators and Prey. Front Behav Neurosci *13*, 60. 10.3389/fnbeh.2019.00060.

Fraser, D., and Rushen, J. (1987). Aggressive behavior. Vet Clin North Am Food Anim Pract *3*, 285-305. 10.1016/s0749-0720(15)31153-1.

Fujita, A., Zhong, L., Antony, M.S., Chamiec-Case, E., Mickelsen, L.E., Kanoski, S.E., Flynn, W.F., and Jackson, A.C. (2021). Neurokinin B-Expressing Neurons of the Central Extended Amygdala Mediate Inhibitory Synaptic Input onto Melanin-Concentrating Hormone Neuron Subpopulations. J Neurosci *41*, 9539-9560. 10.1523/JNEUROSCI.2600-20.2021.

Hashikawa, K., Hashikawa, Y., Tremblay, R., Zhang, J., Feng, J.E., Sabol, A., Piper, W.T., Lee, H., Rudy, B., and Lin, D. (2017). Esr1(+) cells in the ventromedial hypothalamus control female aggression. Nat Neurosci *20*, 1580-1590. 10.1038/nn.4644.

Heiman, M., Kulicke, R., Fenster, R.J., Greengard, P., and Heintz, N. (2014). Cell type-specific mRNA purification by translating ribosome affinity purification (TRAP). Nat Protoc *9*, 1282-1291. 10.1038/nprot.2014.085.

Hunsperger, R.W. (1956). [Affective reaction from electric stimulation of brain stem in cats]. Helv Physiol Pharmacol Acta *14*, 70-92.

Hunsperger, R.W., and Bucher, V.M. (1967). Affective behaviour by electrical stimulation in the forebain and brain stem of the cat. Prog Brain Res *27*, 103-127. 10.1016/s0079-6123(08)63095-2.

Jager, A., Maas, D.A., Fricke, K., de Vries, R.B., Poelmans, G., and Glennon, J.C. (2018). Aggressive behavior in transgenic animal models: A systematic review. Neurosci Biobehav Rev *91*, 198-217.

10.1016/j.neubiorev.2017.09.028.

Jones, L.A., Sun, E.W., Martin, A.M., and Keating, D.J. (2020). The ever-changing roles of serotonin. Int J Biochem Cell Biol *125*, 105776. 10.1016/j.biocel.2020.105776.

Karigo, T., Kennedy, A., Yang, B., Liu, M., Tai, D., Wahle, I.A., and Anderson, D.J. (2021). Distinct hypothalamic control of same- and opposite-sex mounting behaviour in mice. Nature *589*, 258-263. 10.1038/s41586-020-2995-0.

Koolhaas, J.M., Coppens, C.M., de Boer, S.F., Buwalda, B., Meerlo, P., and Timmermans, P.J. (2013). The resident-intruder paradigm: a standardized test for aggression, violence and social stress. J Vis Exp, e4367. 10.3791/4367.

Kretschmer, T., Ouellet-Morin, I., Vrijen, C., Nolte, I.M., and Hartman, C. (2023). Polygenic risk for aggressive behavior from late childhood through early adulthood. Eur Child Adolesc Psychiatry *32*, 651-660. 10.1007/s00787-021-01906-3.

Lee, E.H., Lin, W.R., Chen, H.Y., Shiu, W.H., and Liang, K.C. (1992). Fluoxetine and 8-OH-DPAT in the lateral septum enhances and impairs retention of an inhibitory avoidance response in rats. Physiol Behav *51*, 681-688. 10.1016/0031-9384(92)90103-9.

Li, Y.J., Li, C.Y., Li, C.Y., Hu, D.X., Xv, Z.B., Zhang, S.H., Li, Q., Zhang, P., Tian, B., Lan, X.L., and Chen, X.Q. (2023). KMT2E Haploinsufficiency Manifests Autism-Like Behaviors and Amygdala Neuronal Development Dysfunction in Mice. Mol Neurobiol *60*, 1609-1625. 10.1007/s12035-022-03167-w.

Linnman, C., Moulton, E.A., Barmettler, G., Becerra, L., and Borsook, D. (2012). Neuroimaging of the periaqueductal gray: state of the field. Neuroimage *60*, 505-522. 10.1016/j.neuroimage.2011.11.095.

Lischinsky, J.E., and Lin, D. (2020). Neural mechanisms of aggression across species. Nat Neurosci *23*, 1317-1328. 10.1038/s41593-020-00715-2.

MacLaren, D.A., Browne, R.W., Shaw, J.K., Krishnan Radhakrishnan, S., Khare, P., Espana, R.A., and Clark, S.D. (2016). Clozapine N-Oxide Administration Produces Behavioral Effects in Long-Evans Rats: Implications for Designing DREADD Experiments. eNeuro *3*. 10.1523/ENEURO.0219-16.2016.

Malagie, I., Trillat, A.C., Jacquot, C., and Gardier, A.M. (1995). Effects of acute fluoxetine on extracellular serotonin levels in the raphe: an in vivo microdialysis study. Eur J Pharmacol *286*, 213-217. 10.1016/0014-2999(95)00573-4.

Mar, L., Yang, F.C., and Ma, Q. (2012). Genetic marking and characterization of Tac2-expressing neurons in the central and peripheral nervous system. Mol Brain *5*, 3. 10.1186/1756-6606-5-3.

Miczek, K.A., Maxson, S.C., Fish, E.W., and Faccidomo, S. (2001). Aggressive behavioral phenotypes in mice. Behav Brain Res *125*, 167-181. 10.1016/s0166-4328(01)00298-4.

Motta, S.C., Carobrez, A.P., and Canteras, N.S. (2017). The periaqueductal gray and primal emotional processing critical to influence complex defensive responses, fear learning and reward seeking. Neurosci Biobehav Rev *76*, 39-47. 10.1016/j.neubiorev.2016.10.012.

Nelson, R.J., Demas, G.E., Huang, P.L., Fishman, M.C., Dawson, V.L., Dawson, T.M., and Snyder, S.H. (1995). Behavioural abnormalities in male mice lacking neuronal nitric oxide synthase. Nature *378*, 383-386. 10.1038/378383a0.

Olivier, B., and Mos, J. (1992). Rodent models of aggressive behavior and serotonergic drugs. Prog Neuropsychopharmacol Biol Psychiatry *16*, 847-870. 10.1016/0278-5846(92)90104-m.

Olivier, B., and van Oorschot, R. (2005). 5-HT1B receptors and aggression: a review. Eur J Pharmacol *526*, 207-217. 10.1016/j.ejphar.2005.09.066.

Ota, K.T., Monsey, M.S., Wu, M.S., and Schafe, G.E. (2010). Synaptic plasticity and NO-cGMP-PKG signaling regulate pre- and postsynaptic alterations at rat lateral amygdala synapses following fear conditioning. PLoS One *5*, e11236. 10.1371/journal.pone.0011236.

Park, S.G., Jeong, Y.C., Kim, D.G., Lee, M.H., Shin, A., Park, G., Ryoo, J., Hong, J., Bae, S., Kim, C.H., et al. (2018). Medial preoptic circuit induces hunting-like actions to target objects and prey. Nat Neurosci *21*, 364-372. 10.1038/s41593-018-0072-x.

Qi, G., Zhang, P., Li, T., Li, M., Zhang, Q., He, F., Zhang, L., Cai, H., Lv, X., Qiao, H., et al. (2022). NAc-VTA

circuit underlies emotional stress-induced anxiety-like behavior in the three-chamber vicarious social defeat stress mouse model. Nat Commun *13*, 577. 10.1038/s41467-022-28190-2.

Qin, L., Ma, K., Wang, Z.J., Hu, Z., Matas, E., Wei, J., and Yan, Z. (2018). Social deficits in Shank3-deficient mouse models of autism are rescued by histone deacetylase (HDAC) inhibition. Nat Neurosci *21*, 564-575. 10.1038/s41593-018-0110-8.

Rein, B., Ma, K., and Yan, Z. (2020). A standardized social preference protocol for measuring social deficits in mouse models of autism. Nat Protoc *15*, 3464-3477. 10.1038/s41596-020-0382-9.

Sano, K., Tsuda, M.C., Musatov, S., Sakamoto, T., and Ogawa, S. (2013). Differential effects of site-specific knockdown of estrogen receptor alpha in the medial amygdala, medial pre-optic area, and ventromedial nucleus of the hypothalamus on sexual and aggressive behavior of male mice. Eur J Neurosci *37*, 1308-1319. 10.1111/ejn.12131.

Saudou, F., Amara, D.A., Dierich, A., LeMeur, M., Ramboz, S., Segu, L., Buhot, M.C., and Hen, R. (1994). Enhanced aggressive behavior in mice lacking 5-HT1B receptor. Science *265*, 1875-1878. 10.1126/science.8091214.

Schablon, A., Wendeler, D., Kozak, A., Nienhaus, A., and Steinke, S. (2018). Prevalence and Consequences of Aggression and Violence towards Nursing and Care Staff in Germany-A Survey. Int J Environ Res Public Health *15*. 10.3390/ijerph15061274.

Schreiner, L., and Kling, A. (1953). Behavioral changes following rhinencephalic injury in cat. J Neurophysiol *16*, 643-659. 10.1152/jn.1953.16.6.643.

Shen, F., Wang, N., Qi, C., Li, Y.J., and Cui, C.L. (2014). The NO/sGC/PKG signaling pathway in the NAc shell is necessary for the acquisition of morphine-induced place preference. Behav Neurosci *128*, 446-459. 10.1037/a0036964.

Silva, C., and McNaughton, N. (2019). Are periaqueductal gray and dorsal raphe the foundation of appetitive and aversive control? A comprehensive review. Prog Neurobiol *177*, 33-72. 10.1016/j.pneurobio.2019.02.001.

Stanford, M.S., Houston, R.J., Mathias, C.W., Villemarette-Pittman, N.R., Helfritz, L.E., and Conklin, S.M. (2003). Characterizing aggressive behavior. Assessment *10*, 183-190. 10.1177/1073191103010002009.

Takeda, I., Yoshihara, K., Cheung, D.L., Kobayashi, T., Agetsuma, M., Tsuda, M., Eto, K., Koizumi, S., Wake, H., Moorhouse, A.J., and Nabekura, J. (2022). Controlled activation of cortical astrocytes modulates neuropathic pain-like behaviour. Nat Commun *13*, 4100. 10.1038/s41467-022-31773-8.

Tecott, L.H., and Barondes, S.H. (1996). Genes and aggressiveness. Behavioral genetics. Curr Biol *6*, 238-240. 10.1016/s0960-9822(02)00466-9.

Tovote, P., Esposito, M.S., Botta, P., Chaudun, F., Fadok, J.P., Markovic, M., Wolff, S.B., Ramakrishnan, C., Fenno, L., Deisseroth, K., et al. (2016). Midbrain circuits for defensive behaviour. Nature *534*, 206-212. 10.1038/nature17996.

Vazquez-Leon, P., Miranda-Paez, A., Valencia-Flores, K., and Sanchez-Castillo, H. (2023). Defensive and Emotional Behavior Modulation by Serotonin in the Periaqueductal Gray. Cell Mol Neurobiol *43*, 1453-1468. 10.1007/s10571-022-01262-z.

Vianna, D.M., Borelli, K.G., Ferreira-Netto, C., Macedo, C.E., and Brandao, M.L. (2003). Fos-like immunoreactive neurons following electrical stimulation of the dorsal periaqueductal gray at freezing and escape thresholds. Brain Res Bull *62*, 179-189. 10.1016/j.brainresbull.2003.09.010.

Wall, N.R., Wickersham, I.R., Cetin, A., De La Parra, M., and Callaway, E.M. (2010). Monosynaptic circuit tracing in vivo through Cre-dependent targeting and complementation of modified rabies virus. Proc Natl Acad Sci U S A *107*, 21848-21853. 10.1073/pnas.1011756107.

Wang, W., Schuette, P.J., La-Vu, M.Q., Torossian, A., Tobias, B.C., Ceko, M., Kragel, P.A., Reis, F.M., Ji, S., Sehgal, M., et al. (2021). Dorsal premammillary projection to periaqueductal gray controls escape vigor from innate and conditioned threats. Elife *10*. 10.7554/eLife.69178.

Xu, Y., Lu, Y., Cassidy, R.M., Mangieri, L.R., Zhu, C., Huang, X., Jiang, Z., Justice, N.J., Xu, Y., Arenkiel, B.R., and Tong, Q. (2019). Identification of a neurocircuit underlying regulation of feeding by stress-related emotional responses. Nat Commun *10*, 3446. 10.1038/s41467-019-11399-z.

Yamaguchi, T., Wei, D., Song, S.C., Lim, B., Tritsch, N.X., and Lin, D. (2020). Posterior amygdala regulates sexual and aggressive behaviors in male mice. Nat Neurosci *23*, 1111-1124. 10.1038/s41593-020-0675-x.

Yu, H., Xiang, X., Chen, Z., Wang, X., Dai, J., Wang, X., Huang, P., Zhao, Z.D., Shen, W.L., and Li, H. (2021). Periaqueductal gray neurons encode the sequential motor program in hunting behavior of mice. Nat Commun *12*, 6523. 10.1038/s41467-021-26852-1.

Zelikowsky, M., Hui, M., Karigo, T., Choe, A., Yang, B., Blanco, M.R., Beadle, K., Gradinaru, V., Deverman, B.E., and Anderson, D.J. (2018). The Neuropeptide Tac2 Controls a Distributed Brain State Induced by Chronic Social Isolation Stress. Cell *173*, 1265-1279 e1219. 10.1016/j.cell.2018.03.037.

Zha, X., Wang, L., Jiao, Z.L., Yang, R.R., Xu, C., and Xu, X.H. (2020). VMHvl-Projecting Vglut1+ Neurons in the Posterior Amygdala Gate Territorial Aggression. Cell Rep *31*, 107517. 10.1016/j.celrep.2020.03.081.

Zhang, Q., Hu, D.X., He, F., Li, C.Y., Qi, G.J., Cai, H.W., Li, T.X., Ming, J., Zhang, P., Chen, X.Q., and Tian, B. (2019). Locus coeruleus-CA1 projections are involved in chronic depressive stress-induced hippocampal vulnerability to transient global ischaemia. Nat Commun *10*, 2942. 10.1038/s41467-019-10795-9.

Zhao, Z.D., Han, X., Chen, R., Liu, Y., Bhattacherjee, A., Chen, W., and Zhang, Y. (2022). A molecularly defined D1 medium spiny neuron subtype negatively regulates cocaine addiction. Sci Adv *8*, eabn3552. 10.1126/sciadv.abn3552.

Zhao, Z.D., Yang, W.Z., Gao, C., Fu, X., Zhang, W., Zhou, Q., Chen, W., Ni, X., Lin, J.K., Yang, J., et al. (2017). A hypothalamic circuit that controls body temperature. Proc Natl Acad Sci U S A *114*, 2042-2047. 10.1073/pnas.1616255114.

Zhao, Z.D., Zhang, L., Xiang, X., Kim, D., Li, H., Cao, P., and Shen, W.L. (2023). Neurocircuitry of Predatory Hunting. Neurosci Bull *39*, 817-831. 10.1007/s12264-022-01018-1.